CHEMISTRY
A European Journal

A Journal of
ChemPubSoc Europe

Accepted Article

Title: Mechanistic Insight on the Oxidation of Organic Phenylselenides by H_2O_2

Authors: Giovanni Ribaudo, Massimo Bellanda, Ileana Menegazzo, Lando Peter Wolters, Marco Bortoli, Gerardo Ferrer-Sueta, Giuseppe Zagotto, and Laura Orian

To be cited as: *Chem. Eur. J.* 10.1002/chem.201604915

Link to VoR: http://dx.doi.org/10.1002/chem.201604915

Supported by
ACES

WILEY-VCH

10.1002/chem.201604915

Mechanistic Insight on the Oxidation of Organic Phenylselenides by H_2O_2

Giovanni Ribaudo,[a] Massimo Bellanda,*[b] Ileana Menegazzo,[b] Lando P. Wolters,[b] Marco Bortoli,[b] Gerardo Ferrer-Sueta,[c] Giuseppe Zagotto,[a] and Laura Orian*[a]

[a] Dipartimento di Scienze del Farmaco Università degli Studi di Padova, Via Marzolo 5, 35131 Padova, Italy.

[b]Dipartimento di Scienze Chimiche Università degli Studi di Padova, Via Marzolo 1, 35131 Padova, Italy.

[c] Laboratorio de Fisicoquímica Biológica, Instituto de Química Biológica, Facultad de Ciencias, Universidad de la República, Igua 4225, Montevideo, Uruguay.

laura.orian@unipd.it, massimo.bellanda@unipd.it

Abstract:

The oxidation of organic phenylselenides by H_2O_2 is investigated in model compounds, i.e. *n*-butyl phenyl selenide (**PhSe(n-Bu)**), bis(phenylselanyl)methane (**PhSeMeSePh**), diphenyl diselenide (**PhSeSePh**) and 1,2-bis(phenylselanyl)ethane (**PhSeEtSePh**). Through a combined experimental (^{1}H and ^{77}Se NMR) and computational approach, we characterize the direct oxidation of monoselenide to selenoxide, the stepwise double oxidation of **PhSeMeSePh** leading to different diastereomeric diselenoxides, the complete oxidation of the diphenyldiselenide leading to selenium-selenium bond cleavage and subsequent formation of the phenylseleninic product. Oxidation of **PhSeEtSePh** also results in the formation of phenylseleninic acid along with 1-(vinylseleninyl)benzene which is derived from a side elimination reaction. The evidence of a direct mechanism, in addition to an autocatalytic mechanism, which emerges from kinetic curves, is discussed. By deliberation of observations of diselenides whose chalcogens are separated by alkyl

spacers of different length, a rationale for the advantage of diselenide versus monoselenide catalysts is presented.

Introduction

The reactivity of organoselenium compounds towards peroxides is characteristic of their chemistry, keeping up the pressure on the researchers for this class of compounds for applications in catalysis and biomedicine. [1] H_2O_2 is an environmentally-friendly, commercially inexpensive, easy to handle and oxygen-rich reagent. Despite being thermodynamically favored, the oxidation of organic substrates by H_2O_2 is kinetically unfavorable. [2]

In the late 1970s it was discovered that organoselenium compounds could be efficiently used instead of metals to activate H_2O_2, affording high reactivity and selectivity in numerous organic reactions. Organoselenides are employed as green catalysts in many synthetic transformations, including Baeyer-Villiger oxidations of ketones/aldehydes, the conversion of alkenes to epoxides and the oxidations of alcohols and nitrogen containing compounds. For an exhaustive overview of this class of catalysts the reader is referred to valuable contributions and book chapters written by Braga, Wirth, Santi and Back and co-workers. [1a,2,3]

Upon reaction with H_2O_2, organic monoselenides are oxidized to selenoxides and diselenides are oxidized to seleninic acids via selenoseleninate; the latter inevitably implies cleavage of the selenium-selenium bond. After oxidation, the selenoxide or seleninic acid acts as a peroxide activator, i.e. reacts with H_2O_2 *in situ* to generate hydroxy perhydroxy selenane or peroxyseleninic acid, respectively. These oxygen transfer agents are then able to oxidize organic substrates (Scheme 1).

10.1002/chem.201604915

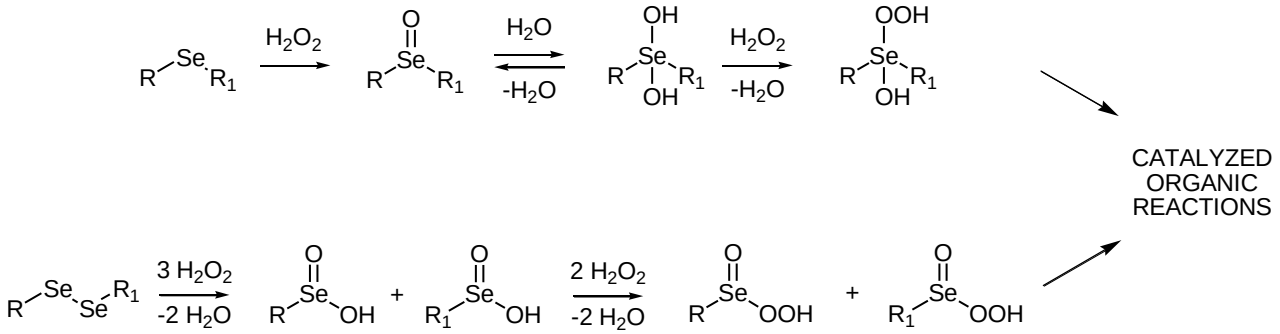

Scheme 1. Oxidation of mono- and diselenides by H_2O_2; R and R_1 are alkyl/aryl groups.

The interest in organoselenides has also animated the biomedical community. The biological role of selenium was assessed in 1973, where it was proven that glutathione peroxidase (GPx) is a selenoprotein, i.e. containing selenium in the form of a selenocysteine (Sec) residue. [4] GPx are a class of enzymes which are ubiquitous in nature, protecting cells from oxidative stress by converting hydrogen peroxide and harmful organic hydroperoxides to water/alcohols. To elucidate the mechanism of the process, a three-step catalytic mechanism has been proposed (i) oxidation of the selenol form of Sec (E-SeH) to a selenenic intermediate (E-SeOH), with simultaneous reduction of one equivalent of hydroperoxide to produce water/alcohol; (ii) reduction of E-SeOH upon reaction with one equivalent of glutathione (GSH), producing water and a selenenyl sulfide intermediate (E-SeSG) and (iii) reduction of E-SeSG by reaction with a second equivalent of GSH to produce the oxidized glutathione (GSSG), resulting in the regeneration of the initial configuration of the enzyme (Scheme 2a).[5] Accidentally, as stressed by Flohé,[6] the first three selenium-enzymes discovered were all peroxidases, which largely influenced the erroneous concept that selenium is *only* a biological anti-oxidant. In contrast, it is important to remember that its presence in 25 human proteins, possessing diversified functions, reveals that selenium also plays other biological roles, which are currently under vigorous investigation. [7]

10.1002/chem.201604915

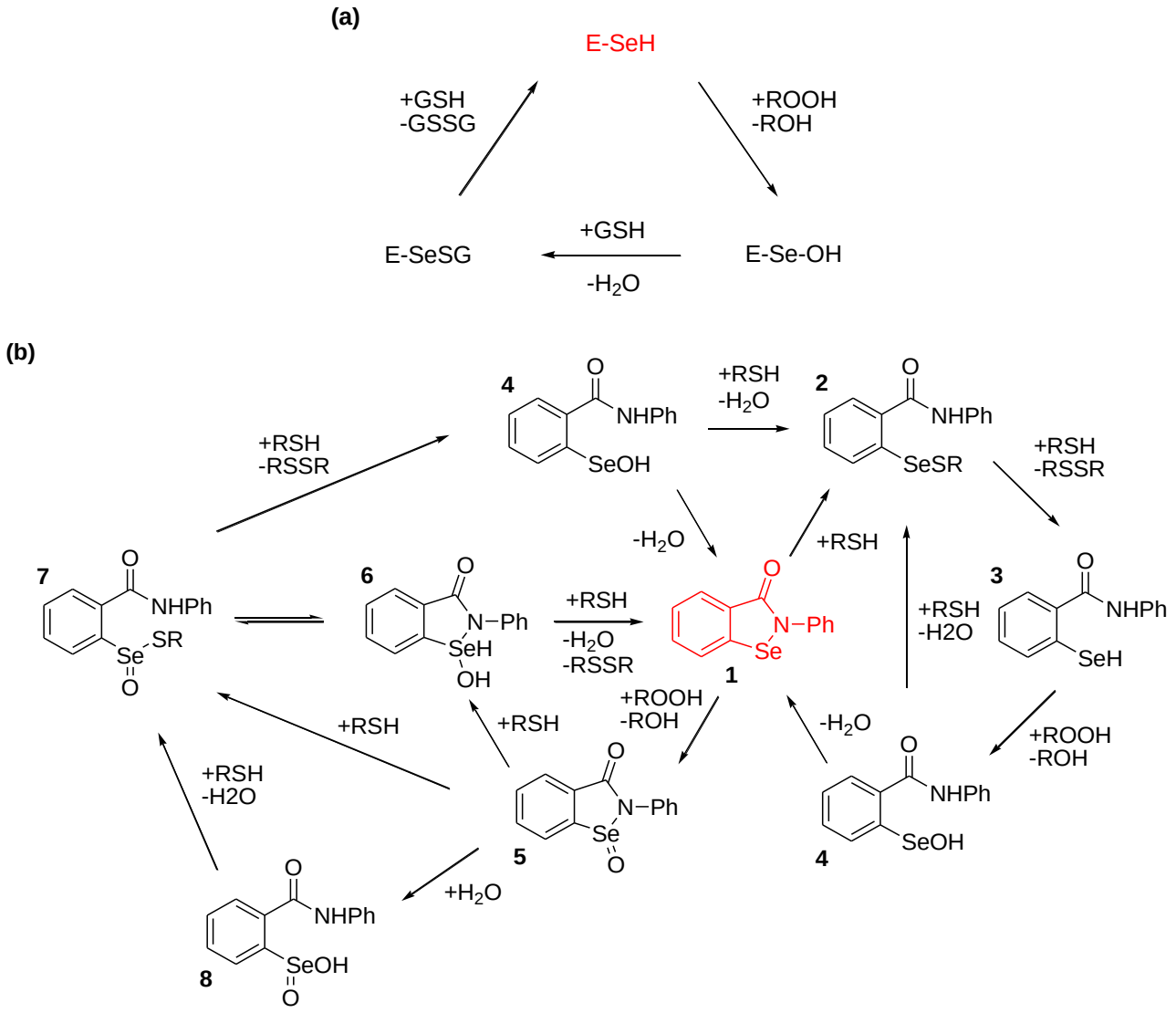

10.1002/chem.201604915

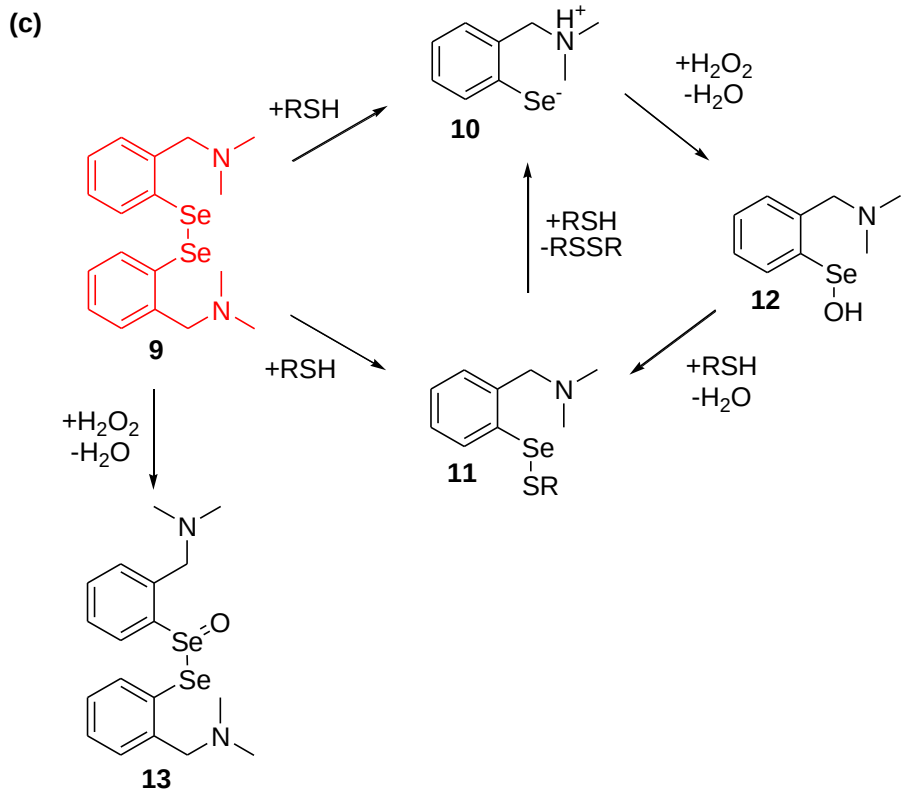

Scheme 2. Catalytic mechanisms of GPx (a) (E represents the enzyme, GSH is glutathione), ebselen (**1**) (b) and N,N-dimethylbenzylamine diselenide (**9**) (c).

GPx's inherent biological activity has inspired the synthesis of organoselenium compounds which could mimic the detoxifying anti-oxidant ability of the enzyme and thus be employed in medicine. [1b,8] The oldest and most popular GPx mimic is ebselen (2-phenyl-1,2-benzisoselenazol-3(2*H*)-one), [9] but so far the mechanistic details of its catalytic activity have not been fully unravelled. Ebselen is a cyclic selenenyl amide (Scheme 2b, **1**) and ring opening is required for the formation of the active selenol species as discerned in the GPx cycle. This can occur via successive reactions with two equivalents of thiol, first forming a selenenyl sulfide (**2**) and then the selenol species (**3**), which subsequently may reduce the peroxide.[10,11] As with GPx, this mechanism is based upon the hypothesis that the selenol is the active reducing agent wherein its oxidation leads to selenenic acid (**4**), an elusive species that has been isolated only in a clathrate.[12] Alternatively, the first step has been proposed to be the reduction of the hydroperoxide forming a seleninyl amide (**5**) whose successive reaction with a thiol may lead to an equilibrium of selenurane (**6**) and seleninyl

sulfide (**7**) as the products, where the latter is monocyclic;[10,11] the conversion of **5** to **7** may also occur stepwise via **8**, where ring opening occurs by hydration. The seleninyl sulfide **7** is then reduced by a second equivalent of thiol to selenenic acid (**4**), which connects it again to the GPx-like cycle described above (Scheme 2b). This mechanism is based on the hypothesis that the reducing agent is a selenenyl amide, the oxidation of which leads to the corresponding seleninyl amide. It has also been suggested that after reduction by thiol with loss of water, the selenurane (**6**) can be converted back to ebselen (**1**) (Scheme 2b). [10,11]

Ebselen is considered as the parent compound of a family of selenenyl amides which have been specifically designed and synthesized to gain an enhanced level of peroxidase activity. [13] Two other classes of GPx mimics, both possessing lesser degree of structural complexity, are intensively studied, i.e. aryl and alkyl monoselenides and aryl diselenides. Compounds of the monoselenide class react with peroxides to form selenoxides. A more complex general mechanism for aryl diselenides has been proposed by Iwaoka and Tomoda. [14] It involves cleavage of the Se-Se bond by reaction with a thiolate, resulting in the formation of a selenenyl sulfide (**11**) and a selenol (**10**), triggering the formerly discussed GPx-like mechanism (Scheme 2c). Alternatively, the diselenide (**9**) has been proposed to react with the peroxide, forming a selenoseleninate (**13**) and water as products (Scheme 2c). The latter step was investigated *in silico* using N,N-dimethylbenzylamine diselenide and it led to a severely distorted structure with an excessively elongated Se-Se bond, thus it was excluded as a possibility.[15] One important advantage of using mono- and diselenides is that they are easier to synthesize than selenenyl amides. In addition to this, the presence of two selenium nuclei undoubtedly enhances the catalytic activity of diselenides, which have received a great deal of attention in the recent years. [16]

On the basis of this *excursus* the significance of the elementary reaction of an organic mono-/diselenide with H_2O_2 (extendable to generic organic hydroperoxides) emerges. To the best of our knowledge, the mechanistic details of the oxidation of organoselenides by H_2O_2 have not been rigorously analyzed and reported yet. Nevertheless, it is worth to mention the contributions of Trout

10.1002/chem.201604915

et al. in their *ab initio* study of the oxidation of organic sulfides by H_2O_2 in aqueous solution, highlighting the role of explicit water molecules in the mechanism of the process. [17]

Contained in this paper is a presentation of the results from combined experimental and theoretical mechanistic investigations concerning the oxidation by H_2O_2 of four organoselenides: *n*-butyl phenyl selenide (**PhSe(n-Bu)**), diphenyl diselenide (**PhSeSePh**), bis(phenylselanyl)methane (**PhSeMeSePh**) and bis(phenylselanyl)ethane (**PhSeEtSePh**) (Figure 1).

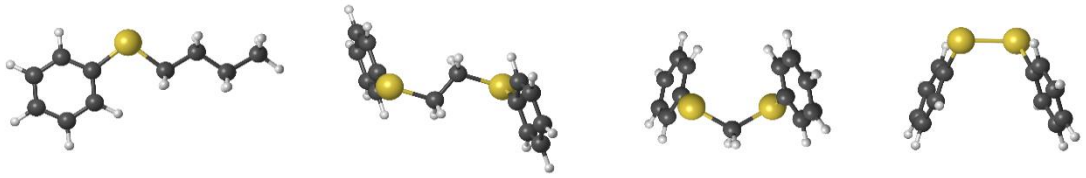

Figure 1. From left to right, molecular geometries of *n*-butyl phenyl selenide (**PhSe(n-Bu)**), 1,2-bis(phenylselanyl)ethane (**PhSeEtSePh**), bis(phenylselanyl)methane (**PhSeMeSePh**) and the global minimum conformation of diphenyl diselenide (**PhSeSePh**); level of theory scalar-ZORA-OLYP/TZ2P-sc.

These compounds were chosen as model organoselenides to allow the comparison of a monoselenide and a diselenide (**PhSe(n-Bu)** and **PhSeSePh**), and to investigate the effect which a spacer of increasing length has upon the reactivity of a diselenide (**PhSeMeSePh** and **PhSeEtSePh**). It is worth to note that **PhSeSePh** itself is a molecule of paramount importance, being widely used as green catalyst as well as a drug, with twice the efficiency of ebselen.[18] For clarity, these four compounds will be referred to in the text using the above described short names; all derivatives will be labelled with progressive numbers as indicated in the schemes.

Materials and Methods

Synthesis. Commercially available chemicals were purchased from Aldrich and used as received, unless otherwise stated. ^{1}H and $^{13}C\{^{1}H\}$ NMR spectra were recorded on a Bruker Avance III 400 MHz spectrometer and on a Bruker AMX 300 MHz spectrometer. All spectra were recorded at room temperature, the solvent for each spectrum is given in parentheses. Chemical shifts are

reported in ppm and are relative to the residual solvent peak. Datasets were edited with Bruker TopSpin suite and iNMR. The multiplicity of signals are reported as singlet (s), doublet (d), triplet (t), quartet (q), multiplet (m), broad (br) or a combination of any of these. High resolution mass spectra (HRMS) were recorded on a ESI-TOF Mariner from Perseptive Biosystem and on a Xevo G2 from Waters, using electrospray (ES) ionization. The purity profile of the compounds was assayed by HPLC using a Varian Pro-Star system equipped with a Biorad 1706 UV-VIS detector and an Agilent C-18 column (5μm, 4.6 x 150 mm). An appropriate ratio of water (A) and acetonitrile (B) was used as mobile phase with an overall flow rate of 1 mL min^{-1}; the general method for the analyses is reported here: 0 minutes (90% A-10% B), 15 minutes (10% A-90% B), 20 minutes (10% A-90% B), 21 minutes (90% A-10% B), 25 minutes (90% A-10% B). The purity of all compounds was ≥ 97%, unless otherwise stated.

General procedure for the preparation of alkyl aryl selenides

Alkyl aryl selenides were prepared according to a procedure reported by Walker *et al.*[19] with minor modifications. Briefly, diphenyl diselenide (0.321 mmol, 1 eq) was dissolved in 10 mL of ethanol. $NaBH_4$ (0.962 mmol, 3 eq) was added over a period of 15 minutes to the solution, which was being stirred in an ice bath. After 30 minutes a solution of the opportune alkyl bromide (0.802 mmol, 2.5 eq) in 2 mL of ethanol was slowly added to the mixture. The resulting solution was allowed to stir at room temperature for an additional 2 hours, after which the solvent was evaporated. The light yellow residue obtained was suspended in diethyl ether (20 mL) and the mixture was washed with water (3 x 10 mL). The organic layer was evaporated to provide the desired alkyl aryl selenide as light yellow oil. Yields: 76-89 %.

*n-butyl phenyl selenide (**PhSe(n-Bu)**)*

R_f=0.76 (hexane); m.p.<25°C; ^{1}H NMR (400 MHz, $CDCl_3$, 25°C): δ=7.46 (m, 2H; PhH), 7.27 (m, 3H; PhH), 2.94 (t, ^3J(H,H)=7.4 Hz, 2H; CH_2), 1.72 (m, 2H; CH_2), 1.45 (m, 2H; CH_2), 0.93 (t,

^{3}J(H,H)=7.4 Hz, 3H; CH_3); ^{13}C NMR (100 MHz, $CDCl_3$, 25°C): δ=132.5, 130.9, 129.1, 126.5, 32.3, 27.7, 23.1, 13.7; ESI-MS: *m*/*z* 215.0339 [M^+] [$C_{10}H_{15}Se^+$]; elemental analysis calcd (%) for $C_{10}H_{14}Se$: C 56.3, H 6.6; found: C 56.3, H 6.6.

n-heptyl phenyl selenide

R_f=0.74 (hexane); ^{1}H NMR (400 MHz, $CDCl_3$, 25°C): δ=7.51 (m, 2H; PhH), 7.27 (m, 3H; PhH), 2.94 (t, ^{3}J(H,H)=7.3 Hz, 2H; CH_2), 1.73 (m, 2H; CH_2), 1.42 (m, 2H; CH_2), 1.4-1.3 (m, 4H; CH_2), 0.93 (t, ^{3}J(H,H)=7.4 Hz, 3H; CH_3); ^{13}C NMR (100 MHz, $CDCl_3$, 25°C): δ=132.4, 130.8, 129.0, 126.6, 31.7, 30.2, 29.8, 28.8, 28.0, 22.6, 14.1; MS: *m*/*z* 257.0803 [M^+] [$C_{13}H_{21}Se^+$]; elemental analysis calcd (%) for $C_{13}H_{20}Se$: C 61.2, H 7.9; found: C 61.3, H 7.9.

n-nonyl phenyl selenide

R_f=0.72 (hexane); ^{1}H NMR (400 MHz, $CDCl_3$, 25°C): δ=7.51 (m, 2H; PhH), 7.26 (m, 3H; PhH), 2.94 (t, ^{3}J(H,H)=7.3 Hz, 2H; CH_2), 1.72 (m, 2H; CH_2), 1.4-1.2 (m, 10H; CH_2), 0.92 (t, ^{3}J(H,H)=7.4 Hz, 3H; CH_3); ^{13}C NMR (100 MHz, $CDCl_3$, 25°C): δ=132.4, 130.7, 128.9, 126.6, 31.9, 30.2, 29.8, 29.4, 29.2, 29.1, 27.4, 22.6, 14.1; MS: *m*/*z* 285.1119 [M^+] [$C_{15}H_{25}Se^+$]; elemental analysis calcd (%) for $C_{15}H_{24}Se$: C 63.6, H 8.5; found: C 63.7, H 8.4.

Synthesis of bis(phenylselanyl)alkanes

Previous reports described the preparation of bis(phenylselanyl)alkanes from diphenyl diselenide under a number of conditions, such as using sodium hydroxide and hydrazine hydrate in N,N-dimethyl-formamide;[20] $RhCl(PPh_3)_3$, hydrogen and triethylamine in tetrahydrofuran;[21] sodium hydroxide, formaldehyde and sodium hydrogen sulfite in ethanol and dichloromethane.[22] While most of the reported procedures require handling of delicate reactants, long reflux times or multi-step reactions,[23,24] we optimized the conditions for the reaction of diphenyl diselenide with sodium borohydride in ethanol to generate a straightforward procedure to obtain the desired compounds in

mild conditions, with a single step, producing good yields. The compounds were prepared following the procedure for alkyl aryl selenides using 1.25 eq of alkyl halide (1,2-dibromo ethane or diiodomethylene) and 5 eq of $NaBH_4$.

*bis(phenylselanyl)methane (**PhSeMeSePh**)*

Yield: 46%. R_f=0.79 (hexane); m.p.<25°C; ^{1}H NMR(400 MHz, $CDCl_3$, 25°C): δ=7.58 (m, 4H; PhH), 7.31 (m, 6H; PhH), 4.29 (s, 4H; CH_2); ^{13}C NMR (100 MHz, $CDCl_3$, 25°C): δ=133.0, 130.8, 129.1, 127.6, 21.0; ESI-MS: *m*/*z* 328.9707 [M^+] [$C_{13}H_{13}Se_2^+$]; elemental analysis calcd (%) for $C_{13}H_{12}Se_2$: C 47.9, H 3.7; found: C 47.8, H 3.7.

*1,2-bis(phenylselanyl)ethane (**PhSeEtSePh**)*

Yield: 32 %. R_f=0.75 (hexane); m.p.<25°C; ^{1}H NMR(400 MHz, $CDCl_3$, 25°C): δ=7.46 (m, 4H; PhH), 7.27 (m, 6H; PhH), 3.16 (s, 2H; CH_2); ^{13}C NMR (100 MHz, $CDCl_3$, 25°C): δ= 133.1, 129.2, 127.7, 127.2, 27.2; ESI-MS: *m*/*z* 342.9501 [M^+] [$C_{14}H_{15}Se_2^+$]; elemental analysis calcd (%) for $C_{14}H_{14}Se_2$: C 49.4, H 4.1; found: C 49.4, H 4.2.

NMR analysis and kinetic studies. NMR experiments were performed at 25°C on a Bruker Avance III 400 spectrometer (400.13 MHz ^{1}H frequency, 100.62 MHz ^{13}C frequency, and 76.37 MHz ^{77}Se frequency) equipped with a 5 mm multinuclear inverse z-field gradient probe-head. For data processing the Topspin 3.5 software was used. The ^{1}H chemical shifts were reported in ppm and referenced to the residual solvent signal. ^{1}H and ^{77}Se resonances assignments were obtained using 2D ^{1}H–^{77}Se heteronuclear multiple-bond correlation (^{1}H–^{77}Se HMBC) experiment with gradient coherence selection. [25] ^{77}Se chemical shifts were referenced to diphenyl diselenide in $CDCl_3$ (463.0 ppm). The ^{1}H–^{77}Se HMBC spectra were acquired using a repetition delay of 1 s; a total of 300 experiments of 16-40 scans were accumulated and processed with a magnitude calculation; 33.3 ms evolution delay was used for ^{1}H–^{77}Se long-range coupling constants; the

spectral width was 13 ppm in F2, 600-1200 ppm in F1. Zero-filling in both F1 and F2 dimensions, multiplication with a Gaussian function (in F2) and a squared sine function (in F1) were performed prior to 2D Fourier Transform. To follow reaction kinetics, compounds (10 mM) were dissolved in 0.5 mL of methanol-D4 before the addition of the opportune amount of H_2O_2 in D_2O (1 or 3 equivalents [26]) several ^1H one-dimensional NMR spectra were recorded with 8 transients, 12 ppm spectral width, and 32k data points. Exponential multiplication with line broadening of 0.3 Hz was applied prior to Fourier Transform.

Computational methodology. All calculations were carried out using the Amsterdam Density Functional (ADF) program developed by Baerends and co-workers [27] and the Quantum-regions Interconnected by Local Descriptions (QUILD) program. [28] The numerical integration was performed using the fuzzy cells integration scheme developed by Becke. [29] The molecular orbitals (MOs) were expanded in a large uncontracted set of Slater type orbitals (STOs, no Gaussian functions are involved). All geometries and energies are obtained using the TZ2P basis set. [30] The TZ2P basis set is of triple-ζ quality for all atoms and has been augmented with two sets of polarization functions. Core shells of the atoms (1s for C and O; up to 3p for Se) were treated by the frozen-core approximation, here denoted '-sc'. NMR chemical shielding constants have been calculated using the all-electron quadruple-ζ quality QZ4P basis set. [30] All calculations include scalar relativistic effects, accounted for using the zeroth-order regular approximation (ZORA). [31]

For the computation of NMR chemical shifts, [32] the geometries and NMR shielding tensors were calculated with the OPBE functional. [33] The scalar-ZORA-OPBE/TZ2P-sc approach has been found to give reliable geometries for the class of compounds in this study. [34]

The shielding constant was in two cases broken down as the sum of a diamagnetic and paramagnetic contribution ($\sigma=\sigma_d+\sigma_p$); the spin-orbit term must also be added, but only when explicitly considered in the calculations, which is not our case. [32,35] The diamagnetic term is almost constant for a given nucleus in different compounds because it depends mainly on the core-shell electrons and cancels out in the chemical shift calculation. The paramagnetic term can be further decomposed as the sum of two terms ($\sigma_p=\sigma_p^{occ\text{-}occ}+\sigma_p^{occ\text{-}vir}$): the former is a sum over all pairs of occupied orbitals; the latter is a sum over all pairs of orbitals consisting of an occupied orbital and virtual orbital; each term is weighted by the inverse of the energy gap and is proportional to the

magnetic coupling between the involved orbitals. $\sigma_p^{occ\text{-}vir}$ is the largest contribution to σ_p and is mostly responsible for the variation in chemical shift. [35]

The energy profiles were obtained from geometries and energies computed using the OLYP functional, [33b,36] which was chosen because it is known to perform well for reactivity studies on organic compounds, [37] and it has been recently benchmarked [34] and applied [38] to organic dichalcogenides. Energy minima and transition states have been verified through vibrational analysis. [39] All minima were found to have zero imaginary frequencies and all transition states have one, corresponding to the mode of the reaction under consideration.

Results and discussion

This section is organized as follows: firstly, the reactivity of the monoselenide is described and discussed; following this, the results pertaining the diselenides in which the chalcogens are separated by methylene and ethylene groups are presented; in the latter case there is a limitation due to the side elimination reaction, which leads to Se-Se bond cleavage and alkene formation; finally, diphenyl diselenide is considered, stressing the mechanistic implications related to the presence of a direct Se-Se bond.

Oxidation of PhSe(n-Bu)

It is well known that arylselenides react with peroxides by undergoing direct oxidation to provide the corresponding selenoxides (Scheme 3a).

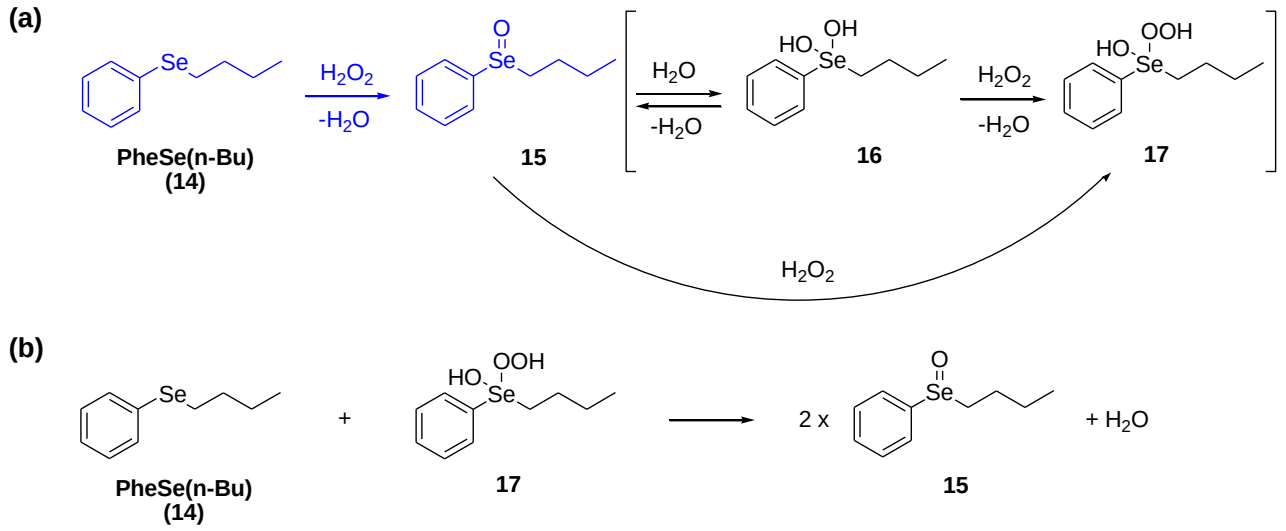

Scheme 3. Mechanism of oxidation of **PhSe(n-Bu)** by H_2O_2. The direct oxidation step is shown in blue.

The reaction of **PhSe(n-Bu)** (**14**) with H_2O_2 in methanol was characterized by ^{1}H and ^{77}Se NMR. A few minutes after addition of H_2O_2 a new set of peaks began to appear, shifted down-field with respect to the original signals, which may be attributed to the selenoxide **15**. Upon oxidation, all methylene multiplets of the butyl chain become more complex due to the fact that the two protons of each CH_2 are no longer equivalent, but diastereotopic. This effect is particularly evident for the methylene groups in α and β position with respect to the Se nucleus, for which two well distinguished signals for each proton can be observed (Figure 2 (d)). The reactants and final products were also characterized by ^{1}H-^{77}Se-HMBC experiments. In general, one expects to observe correlations between the Se nucleus and protons separated by 2 or 3 covalent bonds for these experiments. Indeed, the ^{1}H–^{77}Se HMBC spectrum of **PhSe(n-Bu)** shows three peaks (^{77}Se δ = 290 ppm) corresponding to the correlations with the aromatic protons in ortho and with the methylene protons in α and β positions (Figure 2 (a)) The same pattern of signals was observed for oxidation product **15** at the end of the reaction time, which possessed a much higher ^{77}Se chemical shift (856 ppm) (Figure 2 (b)).; the identity of this species was also confirmed by HRMS analysis on the reaction product (m/z 231.02, Figure S1).

10.1002/chem.201604915

Since ^{77}Se NMR is a very practical tool in the assessment of the oxidation states of Se nuclei, [40] we have systematically measured and calculated the ^{77}Se chemical shifts (Table 1). With the established protocol, i.e. scalar-ZORA-OPBE/QZ4P//scalar-ZORA-OPBE/TZ2P-sc, we found adequate agreement between measured and calculated ^{77}Se δ values, holding true when considering the $\Delta\delta$. Firstly, the calculations do not predict any change in ^{77}Se chemical shift with increasing length of the alkyl chain, in agreement with the experiment. The deviation of approximately 40 ppm from the measured value obtained for **14**, which is within the error typically reported for DFT calculations on Se compounds,[41] may be due to neglecting conformational effects; the error becomes smaller in the oxidized species, which are characterized by possessing a more rigid structure.

It was possible to follow the reaction kinetics of **PhSe(n-Bu)** reacting with H_2O_2 with NMR, due to the fact that the NMR signals of reactants and products do not overlap. In particular, the integrated area of the multiplets corresponding to the aromatic protons and to the CH_2 α protons, which are always well isolated during the reaction, were used to monitor the kinetics (Figure 2 (c) and (d)). During the reaction the disappearance of **14** was closely accompanied by the emergence of **15** (Figure 2 (e)); no other signals were detected in the NMR spectrum, indicating the absence of an intermediate species.

10.1002/chem.201604915

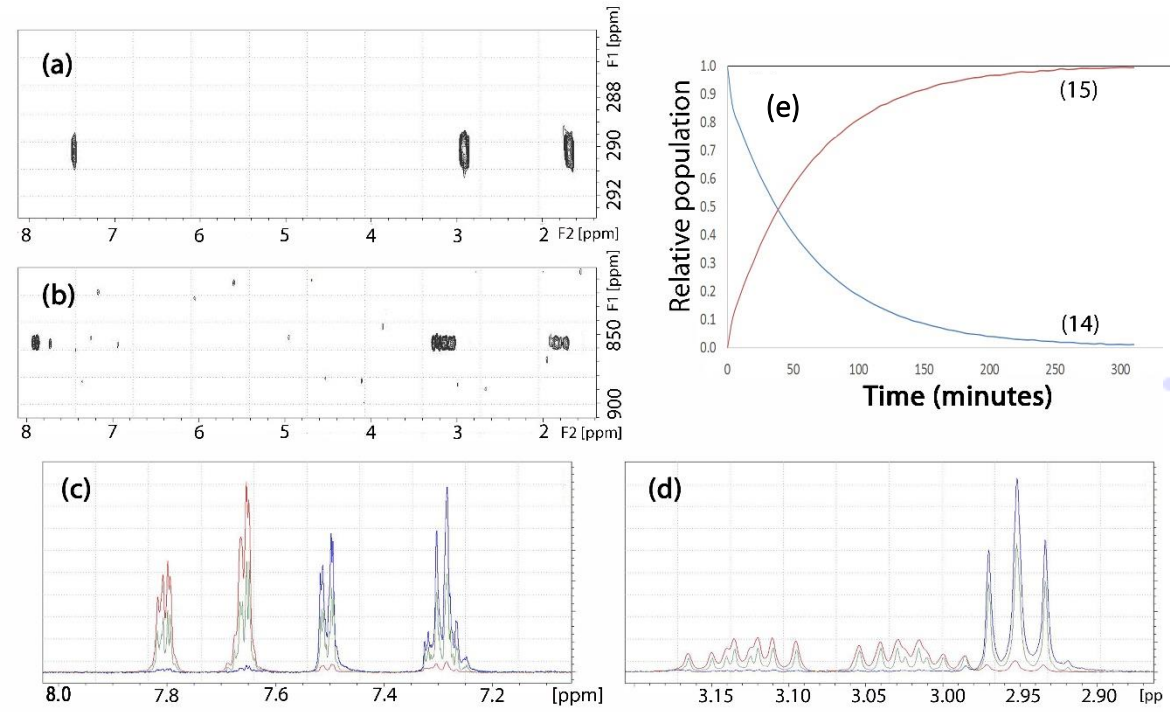

Figure 2. Experimental characterization by NMR of **PhSe(n-Bu)** (10mM) oxidation by 3 equivalents of H_2O_2: ^{77}Se-HMBC of reduced (a) and oxidized (b) **PhSe(n-Bu)**; representative changes in the ^{1}H-NMR for aromatic protons (c) and for the methylene group directly attached to selenium (d), after 4 (blue), 55 (green) and 310 minutes (red) from the addition of H_2O_2. The normalized area of the NMR signals shown in panels (c) and (d), averaged for each compound, have been used to derive the kinetic profile represented in (e); the kinetic curves are labeled with the compound numbers used in the text.

10.1002/chem.201604915

Table 1. Experimental[a] and computed[b] ^{77}Se NMR chemical shifts, in ppm, relative to $(CH_3)_2Se$.

Compound	Alkyl	Exp.	Comp.
n-Alkyl phenyl selenide	Methyl	202,203[c]	193.4
	Ethyl	325,326,327[c],	264.1
	Propyl	288[c]	253.1
	Butyl (**14**)	290[d]	252.9
	Pentyl	292[c]	253.0
	Heptyl	291[d]	252.7
	Nonyl	291[d]	252.9
n-Alkyl phenyl selenoxide	Butyl (**15**)	856[e]	857.0
PhSeEtSePh (**23**)	–	339[d]	360.3
PhSeMeSePh (**18**)	–	345[d]	391.4
PhSe(O)MeSePh (**19**)	–	255 / 867[e]	242.2, 874.2
PhSe(O)MeSe(O)Ph (**20**)	R.R	858[e]	855.6
	R.S		859.9, 868.2
Diphenyl diselenide (**33**)	–	463[d] 456[e]	388.1 / 593.9[f]

[a] Measured at 25°C as described in materials and methods. [b] Computed at scalar-ZORA-OPBE/QZ4P//scalar-ZORA-OPBE/TZ2P-sc. [c] Data from Ref. [42] [d] Solvent: $CDCl_3$ [e] Solvent: MeOD-d4. [f] ^{77}Se chemical shifts for two different stable conformations, see text.

As the product of the reaction between **PhSe(n-Bu)** and H_2O_2 was straightforwardly characterized as **15**, relatively few reaction mechanisms are considered plausible. *In primis*, we explored the direct oxidation, which, based on purely electronic energies, occurs via a reaction barrier of +16.2 kcal mol^{-1}, leading to the selenoxide product **15** at –36.8 kcal mol^{-1}.

According to a mechanistic hypothesis (Scheme 1), [2,43] **15** can subsequently react with H_2O, to form a dihydroxy product (**16**). This reaction involves a transition state (TS) at +22.8 kcal mol^{-1}, after which the product is obtained at +13.1 kcal mol^{-1} (among the conformers we considered the most stable product, which has two hydroxy groups at roughly a 180º angle). From **16**, the hydroxy perhydroxy selenane **17** can be formed upon reaction with H_2O_2, which lies at +3.3 kcal mol^{-1}; for this step a barrier of +15.6 kcal mol^{-1} has been computed (Scheme 3a). The possibility of a direct conversion of **15** into **17** was explored, which is suggested to form, after addition of a second equivalent of H_2O_2, via a transition state at +15.0 kcal mol^{-1} (relative to **14** and H_2O_2, Scheme 3a). Several conformations were also located for this product. Presumably, the hydroxy

10.1002/chem.201604915

perhydroxy selenane will initially form in a conformation which has the hydroxy- and perhydroxy-substituents approximately orthogonal to each other, at a relative energy of +13.9 kcal mol^{-1}. However, the species with these substituents at a 180° angle (in plane with the phenyl ring) was found to be the minimum energy structure, being more than 10 kcal mol^{-1} lower in energy, at +3.3 kcal mol^{-1}. On the basis of the energetics, we therefore assume that the transition from the selenoxide **15** to **17** is more likely to occur in one step, *i.e.*, addition of H_2O_2. **17** is considered to be the active oxidant species in numerous Se-catalyzed organic reactions. In addition, the hydroxy perhydroxy selenane itself might act as an oxidant towards **14**, reacting with one equivalent of the starting compound (Scheme 3b). In this reaction, an oxygen atom from the perhydroxy group is transferred to **14**, forming the selenoxide product **15**, and the remaining hydroxy group leaves together with the hydrogen from the perhydroxy group to form water, thereby generating a second equivalent of **15**. The computed energy barrier for this reaction is +23.6 kcal mol^{-1}, with the products having a relative energy of –40.1 kcal mol^{-1}. On the basis of the energetics, and largely due to the lack of evidence for an autocatalytic mechanism in the kinetic profile (Figure 2 (b)), this oxidation mechanism for **14** was ruled out.

Oxidation of PhSeMeSePh and oxidation of PhSeEtSePh

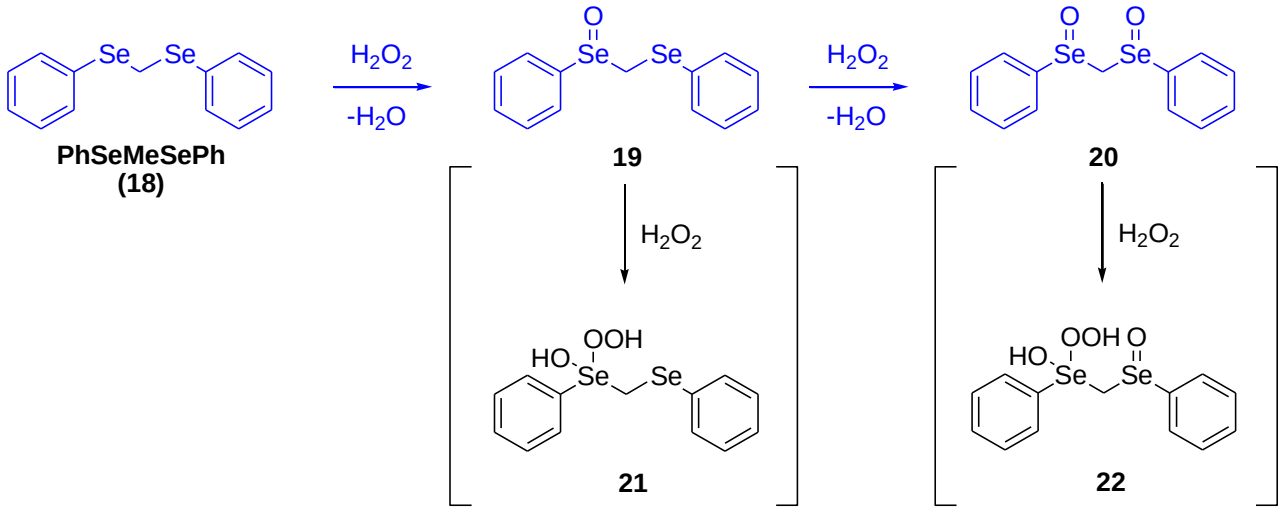

Scheme 4 Mechanism of oxidation of **PhSeMeSePh** by H_2O_2. The direct oxidation step is shown in blue.

10.1002/chem.201604915

As with **PhSe(n-Bu)**, the combination of ^{1}H and ^{77}Se NMR proved to be a useful tool in the characterization of the reaction between **PhSeMeSePh** (**18**) and H_2O_2. The ^{1}H–^{77}Se HMBC spectrum of **18** shows a single group of signals (^{77}Se δ=343 ppm), as expected for a fully reduced symmetric dinuclear selenide. When the oxidation was carried out using one equivalent of H_2O_2, two distinct sets of peaks were observed in the selenium dimension, at 255 ppm and at 867 ppm, compatible with the presence of a reduced and an oxidized Se nucleus, respectively (Figure 3 (a)). Interestingly, only very weak signals were detected at the Se frequency for the initial unoxidized. The new signal at 255 ppm was assigned to the reduced selenium atom of **19**, which despite being close to a seleninyl group, appears to be strongly shielded; this up-field shift is also supported by DFT calculations (*vide infra*). As the two groups of signals at 255 and 867 ppm have approximately the same intensity, we can ascertain that only the mono-oxidized product **19** was formed. The identity of **19** was confirmed also by HRMS analysis on the reacted sample (m/z 342.93, Figure S2).

10.1002/chem.201604915

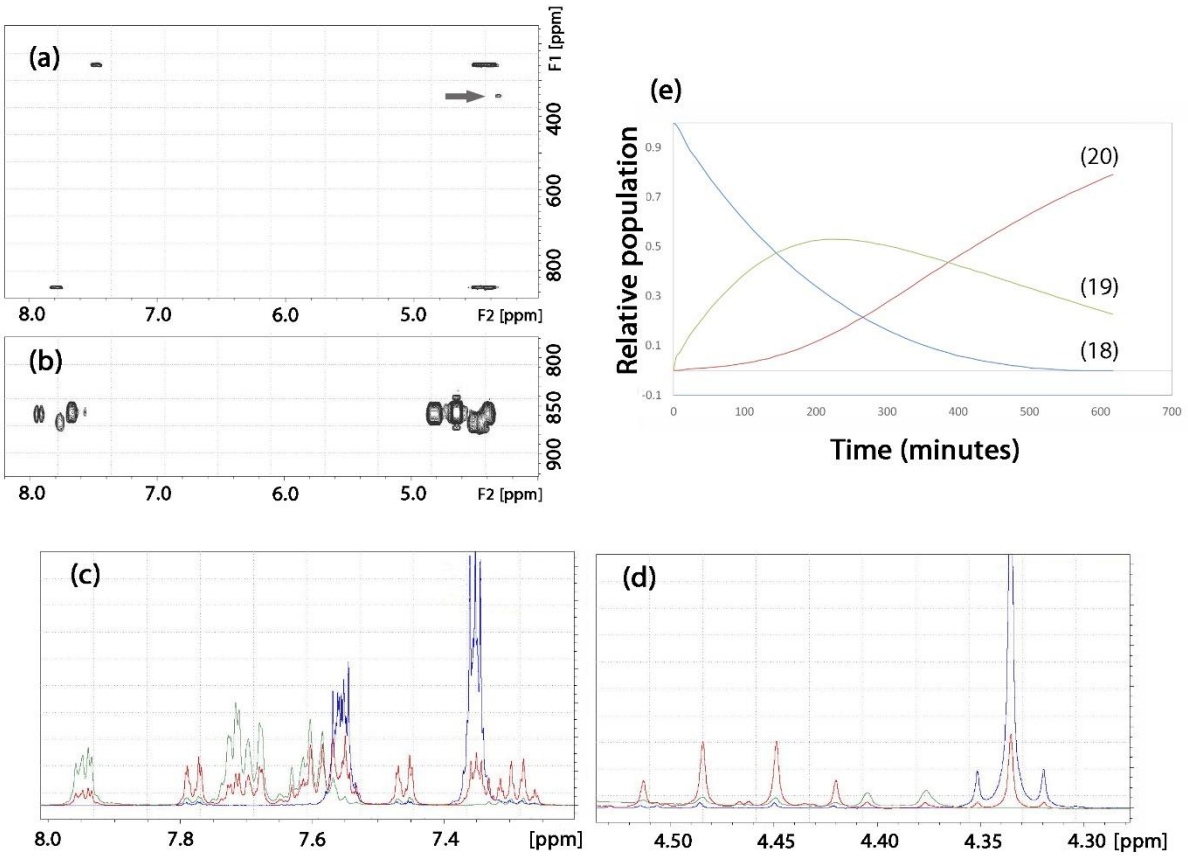

Figure 3. Experimental characterization by NMR of **PhSeMeSePh**(10mM) oxidation by H_2O_2: ^{77}Se-HMBC of **PhSeMeSePh** oxidized by 1 equivalent of H_2O_2 (a) and by 3 equivalents of H_2O_2 (b); the weak signal at 343 ppm, indicated by the arrow derive from a small amount of unreacted starting reagent. For the reaction using 3 equivalents of H_2O_2, representative changes in the ^{1}H-NMR for aromatic protons (c) and for the methylene bridge (d), after 4 (blue), 295 (green), and 845 minutes (red) are shown. The two sidebands around the peak at 4.34 ppm derive from the scalar coupling with natural abundance of ^{77}Se. The normalized areas of selected NMR signals have been used to derive the kinetic profile represented in (e); the reaction was monitored regularly up to 617 minutes and a single spectrum at 845 minutes was recorded to verify that the reaction had reached completion (not included in the kinetic profile); the kinetic curves are labeled with the compound numbers used in the text.

The deduction that the addition of 1equivalent of H_2O_2 leads only to the formation of the mono-oxidized species **19** is also inferred by the results obtained by the oxidation of **18** by 3 equivalents of H_2O_2 (Figure 3 (b)). Using these conditions in conjunction with the ^{1}H–^{77}Se HMBC experiment, a new set of signals appeared at 858 ppm, a value seen to be shifted only slightly up-field with respect to the spectrum of **19**. However, the peaks at ^{77}Se δ= 858 ppm cannot be assigned to a single molecular form. Specifically, there was an observation of two peaks in the aromatic region (correlation with protons in ortho to Se nucleus) and three peaks in the aliphatic region

(correlations with methylene protons) (Figure 3 (b)). Despite this observation in the NMR spectrum, HRMS confirmed the exclusive presence of the diselenoxide form (m/z 360.93, Figure S2). In order to fully comprehend this behavior, the reaction product obtained from the oxidation of **18** by 3 eq. of H_2O_2 was analyzed by HPLC-DAD, revealing the formation of two diasteroisomers, namely (*R,R*)-**20** (or (*S,S*)-) and (*R,S*)-**20**. Also in support of this argument, is the identification of two species exhibiting superimposed UV spectra in the chromatogram. Furthermore, the relative abundance of the two diasteroisomers was estimated to be approximately 6:5, fully consistent with the observations by ^{1}H NMR, discussed below (Figures S5, S6 and S7). Notably, similar spectral behavior has previously been reported for optically active disulfoxides. [44]

Considering the use of 3 equivalents of H_2O_2, the kinetics for the complete oxidation of **18** to the di-oxidized species **20** was fully characterized by 1D ^{1}H NMR. This was possible because all involved species (Scheme 4) possess at least one signal well separated from those of the others (Figure 3 (c) and (d)). The disappearance of **18** was followed by monitoring the singlet at 4.34 ppm, which corresponds to the two equivalent protons of the methylene bridge. The protons become dissimilar after one Se nucleus is oxidized to form **19**, causing the NMR signal to be split into a second order doublet of doublets centred at 4.46 ppm. The intensity of this signal increases throughout the duration of the reaction in parallel with those of the multiplets at 7.48 and 7.79 ppm, which were unambiguously assigned with the ^{1}H–^{77}Se HMBC experiments as aromatic protons in ortho position to the reduced and oxidized Se nuclei of **19**.

Upon treatment with approximately 1 equivalent of H_2O_2, the conversion of the initial product to **19** reached about 90% and then very slowly it started to decrease accompanied by the appearance of new signals which may be attributed to **20**, and **19** remained as the predominant species (>80%, not shown). The kinetic profile obtained using 3 equivalents of H_2O_2 shows that **19** reached a maximum conversion of approximately 55% and then was further oxidized to **20**, which remained as the major product at the end of the reaction (Figure 3 (e)). The NMR experiments clearly show that two different products were obtained at completion of the reaction. As mentioned

above, three different signals are present in the spectral region between 4.4 and 4.8 ppm: two doublets characterized by the same splitting of 11.2 Hz and centered at 4.39 ppm (Figure 3 (d)) and 4.82 ppm and a triplet at 4.65 ppm (not shown). The two doublets are assigned to the methylene protons of the (*R*,*S*)/(*S*,*R*) diasteromeric forms, which are predicted, at scalar-ZORA-OPBE/QZ4P//scalar-ZORA-OPBE/TZ2P-sc, to have very different chemical shift values ($\Delta\sigma$=1.1ppm), while the triplet is assigned to a second order spin system for the methylene in which the two protons resonate at a very similar frequency, in accordance with the computations which reveal two symmetry-equivalent methylene protons both in the (*R*,*R*), and the (*S*,*S*) form.

Unfortunately, the two signals at lower field overlap with the strong, broad solvent signal, meaning the relative quantities of the two diasteroisomers could not be discerned from them. However, it was possible to estimate this integration of the multiplets in the aromatic region at the end of the reaction (Figure 3 (c)). The relative areas of the three groups of signals centered at 7.93, 7.67 and 7.58 ppm are 4.0, 10.9 and 7.5, respectively, and they can be rationalized only assuming a ratio of 6:5 between the diasteroisomers, whose signals partially overlap (4.0:6+(4x1.2):6x1.2).

Computed ^{77}Se chemical shifts for compounds **18**-**20** are in agreement with experimental values (Table 1); in particular, upon mono-oxidation the ^{77}Se NMR δ of the oxidized chalcogen is shifted down field by almost 500 ppm, while the ^{77}Se NMR δ of the unoxidized nucleus unexpectedly decreases by approximately 150 ppm: the initial values change from 391.4 ppm to 874.2 and 242.2 ppm, respectively. In **20**, the two ^{77}Se NMR chemical shifts are almost identical and have the characteristic value measured for a selenoxide, i.e. 855.6 ppm for (*R*,*R*)-**20** and slightly different shifts of 859.9 and 868.2 ppm for the Se nuclei in (*R*,*S*)-**20**, which are not symmetry-equivalent. The decrease in the ^{77}Se chemical shift for the non-oxidized Se nucleus in **19**, detected also experimentally, can be qualitatively rationalized by investigating the transitions between occupied and virtual MOs that contribute most to $\sigma_p^{occ\text{-}vir}$, which in turn constitutes the more important part of the paramagnetic part (σ_p) of the shielding constants. The idea behind this

approach is that the field-induced magnetic moment in a molecule increases if, after applying the magnetic field operator $\hat{B}$ on an occupied orbital, the resulting function overlaps well with an unoccupied orbital in the molecule. Each contributing term to $\sigma_p^{occ\text{-}vir}$ is proportional to this magnetic coupling between occupied and unoccupied MOs and inversely proportional to their energy difference. Taking **18** as reference, it is evident that the up-field shift of the reduced Se nucleus in **19** derives entirely from σ_p, as σ_d is essentially the same for **18** and **19** (it is also worth noting that less negative σ_p values imply larger σ values, i.e. smaller chemical shift values); the data is summarized in Table 2.

Table 2 Decomposition of the shielding constant σ into diamagnetic (σ_d) and paramagnetic (σ_p) components, as well as selected contributions from occupied-virtual orbital transitions to the paramagnetic part of the shielding constant and related orbital energy differences for the reduced Se nuclei in **18** and **19**; all σ values are in ppm and only contributions above 70 ppm are shown. MOs of **18** and **19** involved in the listed transitions are shown in Scheme S4.

			σ	σ_d	σ_p	Selected contributions to $\sigma_p^{occ\text{-}vir}$	$\Delta E^{occ\text{-}vir}$ (eV)
	18		1306.7	2995.4	-1688.7		
HOMO	→	LUMO				-207.0	3.23
HOMO	→	LUMO+4				-114.6	4.41
HOMO	→	LUMO+5				-199.9	4.53
HOMO	→	LUMO+6				-83.2	4.54
HOMO	→	LUMO+7				-92.8	4.80
HOMO-1	→	LUMO+6				-71.6	4.93
HOMO-1	→	LUMO+11				-77.5	5.65
HOMO-6	→	LUMO+11				-74.8	7.78
						Sum: -921.4	
	19		1454.7	2995.2	-1540.5		
HOMO	→	LUMO				-73.3	3.33
HOMO	→	LUMO+5				-73.7	4.62
HOMO	→	LUMO+7				-91.8	4.75
HOMO-1	→	LUMO+7				-107.0	5.21
HOMO-7	→	LUMO+4				-138.8	7.19
HOMO-7	→	LUMO+10				-98.0	7.98
						Sum: -582.6	

In both cases, the sum of the terms contributing to $\sigma_p^{occ\text{-}vir}$ converges slowly, but more so in **19** than in **18**. For both compounds the dominant terms are found between MOs whose energy separation is below 8.0 eV. An analysis of all the involved couples is beyond the scope of this work (isodensity

10.1002/chem.201604915

plots are available in Scheme S4); however, it is illustrative to examine just the HOMO-LUMO transition. This constitutes the largest contribution to the σ_p of **18**, but when compared to **19**, its value of $\sigma_p^{\text{HOMO-LUMO}}$ is more than halved. As the energy gaps are similar (3.23 vs 3.33 eV), the origin of this discrepancy can be found in the change of the value of the integral $\langle\varphi_{LUMO}|\hat{B}|\varphi_{HOMO}\rangle$, where $\hat{B}$ is the magnetic field operator, which is proportional to the angular momentum operator; the effect of $\hat{B}$ upon an atomic p orbital (AO) typically results in a rotation of 90º.[35] In **18**, coupling necessarily occurs through the common lobes located on the Se nuclei (the HOMO has Se p_z / Se p_x character, 41.5% and 42.4% on the two chalcogens, respectively), and upon application of the field operator they gain the required symmetry to overlap with the Se p_x / Se p_z lobes of the LUMO (4.8% and 5.1% on the two chalcogens; the LUMO has also important phenyl character). In **19** however, there is a significant change in the HOMO due to the presence of oxygen; its composition is dominated by Se (oxidized) p_x /p_y / Se (reduced) p_x / O p_x /p_y (6.1%, 35.1% and 33.6%, respectively), while in the composition of the LUMO one finds Se (oxidized) p_x / Se (reduced) p_z / O p_x (3.6%, 4.4% and 1.2%, respectively). Upon application of the field operator to the HOMO, only the lobes found on the reduced Se nucleus gain the necessary symmetry to overlap with the LUMO. This subsequently results in a net decrease of the magnetic coupling and, in absolute terms, of the $\sigma_p^{\text{HOMO-LUMO}}$ in **19**.

Mechanistically, the first oxidation of **PhSeMeSePh** by H_2O_2 was computed to occur via a reaction barrier of +17.2 kcal mol^{-1} and to have a reaction energy of –36.8 kcal mol^{-1}. By reaction with another equivalent of H_2O_2, **19** becomes the doubly oxidized product **20**, existing either as (*R*,*R*)-**20** or (*R*,*S*)-**20** (Figure 4). We do not consider the pathways involving (*S*,*S*)-**20** since it is energetically equivalent to the pathways involving (*R*,*R*)-**20**.

10.1002/chem.201604915

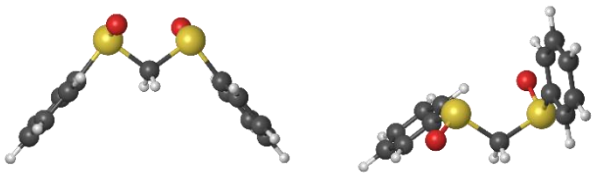

Figure 4. Molecular geometries of (*R*,*R*)-**20** (left) and (*R*,*S*)-**20** (right), optimized at scalar-ZORA-OLYP/TZ2P-sc.

From the calculations it was found that the formation of (*R*,*S*)-**20** goes via a lower reaction barrier (+17.5 kcal mol^{-1}, vs. +18.5 kcal mol^{-1} for (*R*,*R*)-**20**), leading to only a slightly less stable product: –34.2 kcal mol^{-1} vs. –34.4 kcal mol^{-1}. These numbers were generated for the products in their lowest-energy conformations. Other possible configurations, obtained by rotations around the selenium-methylene bonds, are typically all very close in energy.

Also in this case we have explored an alternative route in the reaction between **19** and a second equivalent of H_2O_2, wherein a hydroxy perhydroxy intermediate **21** is formed; for this path, a TS at +14.6 kcal mol^{-1} and a reaction energy of +5.8 kcal mol^{-1} were found (Scheme 4). A catalytically active hydroxy perhydroxy species **22** can be generated also from the fully oxidized product **20** ($\Delta E^{\ddagger}$ = +16.5 kcal mol^{-1}, ΔE = +1.8 kcal mol^{-1}, Scheme 4). The reactions involving these species are shown and commented in the Supporting information (Scheme S1). On the basis of the energetics, the direct oxidation is the favoured mechanism, in agreement with the experimental kinetics, in which there is no evidence for the presence of autocatalytic mechanisms.

In **PhSeEtSePh** (**23**), the longer alkyl bridge imposes a larger distance between the Se nuclei than in **PhSeMeSePh**. After initial oxidation and due to the presence of β protons, a fast elimination reaction takes place leading to monoselenides and olefins as products.

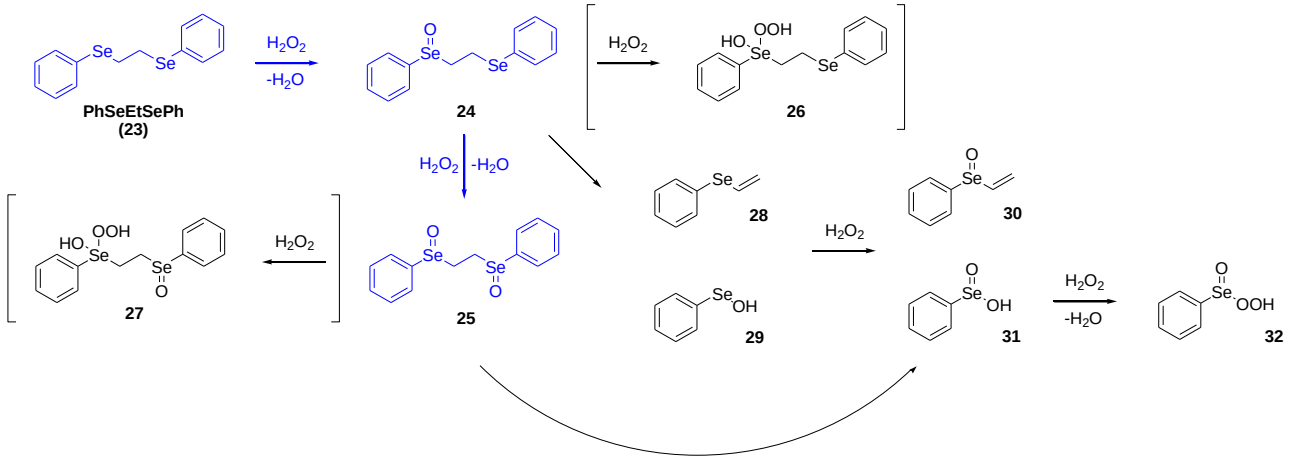

Scheme 5 Mechanism of oxidation of **PhSeEtSePh** by H_2O_2. The direct oxidation step is shown in blue.

The first $^{1}H–^{77}Se$ HMBC spectrum (Figure 5 (a)), the acquisition of which started around five hours after the addition of H_2O_2, was of lower quality with respect to those measured for **PhSe(n-Bu)** and **PhSeMeSePh** in analogous conditions and showed the presence of several groups of weak signals at different ^{77}Se δ. Notably, if the spectrum was Fourier transformed during its acquisition, changes in the relative populations of the different species were observed suggesting that the reaction was still in slow progress. The peaks detected in the ^{77}Se spectrum at frequencies of 334, 320, 863, 868 and 850 ppm were assigned to **PhSeEtSePh**, the reduced and oxidized selenium nuclei of **24**, **25** and **30**, respectively. No correlations between a reduced selenium and the alkene protons were detected, indicating that the mono-oxidized product of the first step (**24**) did not undergo β-elimination to form **28**. As expected, other $^{1}H–^{77}Se$ HMBC experiments acquired at different times during the reaction showed a variation of the relative populations of the different species; this finally lead to the appeareance of a peak at 1158 ppm corresponding to the seleninic acid **31** (Figure 5 (b)), which was confirmed by subsequent HRMS analysis. Despite the relative complexity of the reaction, its kinetic profile could be derived by proton NMR. The starting reagent **PhSeEtSePh** could be monitored by following the changes in the area of the singlet at 3.14 ppm, assigned to the four equivalent protons of the ethylene bridge (Figure 5 (e)). When the first

10.1002/chem.201604915

selenium is oxidized to give **24**, this singlet becomes a complex pattern of signals characterized by three multiplets at 2.98, 3.23 and 3.40 ppm with relative areas of 1:2:1 (Figure 5 (e)). The multiplet at 3.23 ppm was used to follow **24** during the reaction. The protons of the ethylene bridge of **25** result in two multiplets of comparable intensities, at 2.95 and 3.50 ppm; the latter signal remains isolated during the reaction, making it possible to use it as a probe in monitoring **25**. Finally, by integration of the signals at 6.34 and 7.09 ppm, correspond to the alkene protons in β and α positions with respect to Se, respectively, the formation of **30** could be followed.

The kinetic profile is shown in (Figure 5 (f)). Directly after the addition of H_2O_2, **PhSeEtSePh** started to disappear whilst **24** formed at a similar rate. At about 200 minutes **24** reached a maximum conversion of approximately 80%, where its concentration remained constant. At this point **23** continued to decrease along with a relatively slow formation of both **25** and **30**. At ~380 min a sharp acceleration in the disappearance of **24** is observed; this was accompanied by a proportionate increase in the concentration of **25**. However, the relative concentration of **25** quickly diminished due to a β-elimination reaction, resulting in the rapid formation of the alkene **30**, whose concentration shares an inverse relationship with **24** and **25** after approximately 400 min, and the seleninic acid **31,** which may be further oxidized to form **32**. HRMS analysis confirmed the identity of the **24**, **25** and **30** (m/z 358.94, 374.94 and 200.99, respectively; Figure S3). **30** was also identified (m/z 200.99). Notably, there is evidence of autocatalysis in this mechanism, but only in the second part of the process: the onset of the sigmoidal profile is rationalized through the computational mechanistic investigation.

10.1002/chem.201604915

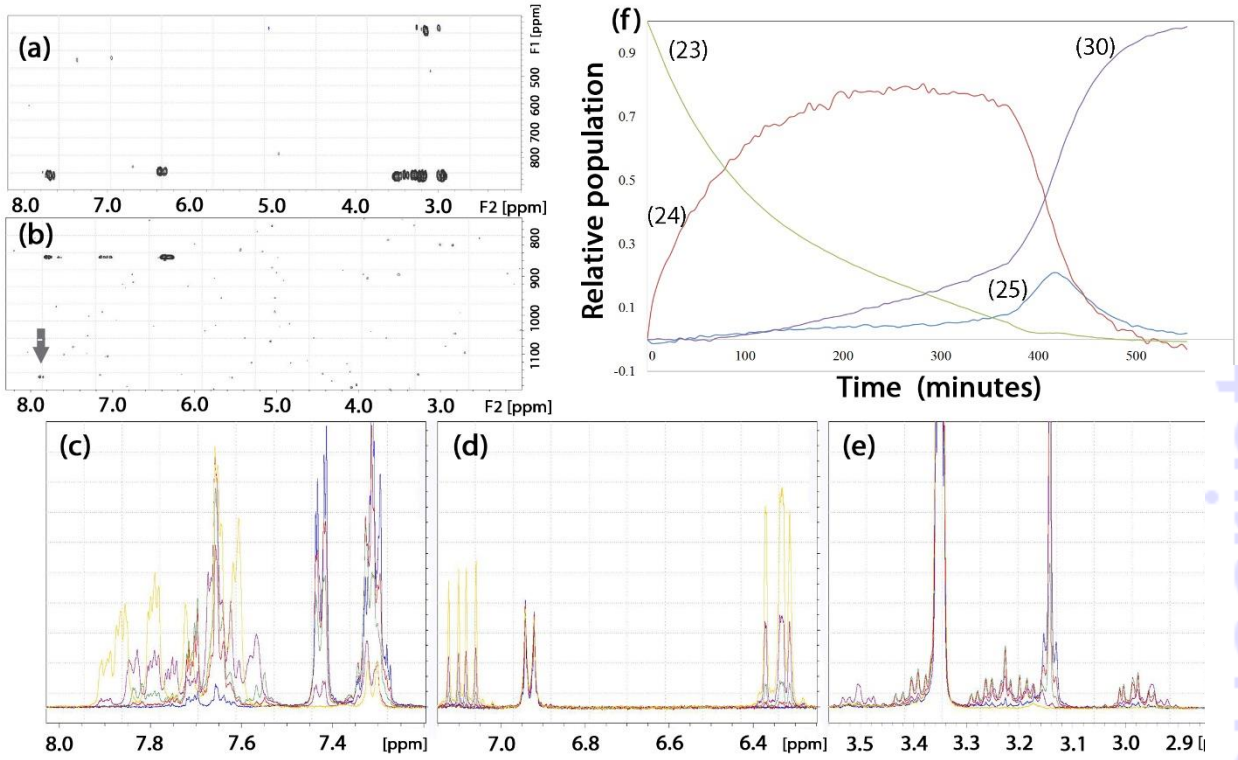

Figure 5. Experimental characterization by NMR of **PhSeEtSePh** (10mM) oxidation by 3 equivalents of H_2O_2: ^{77}Se-HMBC of **PhSeEtSePh** 5 hours after addition of H_2O_2 (a) and at the end of the reaction (b) with H_2O_2; representative changes in the ^{1}H-NMR in the aromatic (c) and alkene regions (d) and in the ethylene bridge (e), after 5 (blue), 105 (red), 257 (green), 410 (purple), and 552 minutes (yellow) from the addition of H_2O_2. The two sidebands around the peak at 3.14 ppm derive from the scalar coupling with natural abundance of ^{77}Se. The normalized areas of selected NMR signals have been used to derive the kinetic profile represented in (f); the kinetic curves are labeled with the compound numbers used in the text.

In silico, the reaction of **23** with the first equivalent of H_2O_2 (Scheme 5) leads to the mono-oxidized product **24**. For this step, the incoming H_2O_2 may approach the Se nucleus from either above or below (referring to the Se nucleus on the left hand side in Fig. 1). The transition states for these two possibilities are very close in energy: the barrier for H_2O_2 approaching from the same side as the ethylene bridge is pointing, is only 0.1 kcal mol^{-1} higher in energy, at +17.4 kcal mol^{-1}. However, the product from this higher-energy TS, with the doubly bonded oxygen and the ethylene C–C bond in approximately eclipsed positions, is 1 kcal mol^{-1} more stable (–35.8 kcal mol^{-1} vs. –34.8 kcal mol^{-1}). In the second oxidation of the second Se center, we again discovered that the lowest-energy pathway is obtained when the doubly-bonded oxygen already present is in a roughly

10.1002/chem.201604915

eclipsed position with respect to the ethylene bridge. In the following discussion, we therefore only consider the pathway for the first oxidation where the H_2O_2 approaches on the side in which the ethylene bridge is pointing ($\Delta E^{\ddagger}$ = +17.4 kcal mol^{-1}, ΔE = –35.8 kcal mol^{-1}).

From the acquired product **24**, reaction with a second equivalent of H_2O_2 can generate the doubly oxidized species **25**. Again, the incoming H_2O_2 has a choice between two sides to approach from, giving either (*R*,*R*)-**25** or (*R*,*S*)-**25** (we do not consider the pathway leading to (*S*,*S*)-**25**, as it is energetically equivalent to that of (*R*,*R*)-**25**). The lowest-energy pathway is obtained when H_2O_2 comes from the side in which the ethylene bridge is pointing, *i.e.*, from below in Figure 1 for the Se nucleus on the right; this route involves a reaction barrier of +17.0 kcal mol^{-1} (relative to **24** and H_2O_2), and leads to the formation of (*R*,*S*)-**25** and water at a relative energy of –36.7 kcal mol^{-1}. Alternatively, with a slightly higher barrier of +18.0 kcal mol^{-1}, H_2O_2 has the option of approach from the opposite side, and this leads to the formation of (*R*,*R*)-**25** at –35.0 kcal mol^{-1}. The reactions involving the hydroxyl perhydroxy species **26** and **27** are shown and commented in the Supporting information (Scheme S2); by analogy with the monoselenide, we consider that overall oxidation by H_2O_2 is energetically more favorable and relatively uncomplicated from a mechanistic viewpoint, inferring that this route is more probable for the reaction.

An interesting observation was made for the doubly oxidized product **25**, for which a β-elimination reaction is observed to take place. As shown in Scheme 5, this produces 1-(vinylseleninyl)benzene (**29**) and benzeneseleninic acid (**31**). The reaction barrier for this step is +19.5 kcal mol^{-1}, leading to the products at +0.6 kcal mol^{-1}. β-elimination of the mono-oxidized product **24**, generating the alkenes **28** and **29**, results in the calculation of a higher barrier of +21.2 kcal mol^{-1}; this presumably prevents this reaction from occurring, despite possessing a favorable reaction energy of –3.0 kcal mol^{-1}. In addition, the latter reaction would subsequently be followed by oxidation of **28** to **30** ($\Delta E^{\ddagger}$ = +19.3 kcal mol^{-1}, and ΔE = –33.1 kcal mol^{-1}). For both β-elimination reactions, the resulting phenyl selenenic acid **29** undergoes a successive reaction with

H_2O_2 to form the benzeneseleninic acid **31**; this step is seen to have a relatively low reaction barrier of +12.6 kcal mol^{-1} and a large negative reaction energy of –49.2 kcal mol^{-1}. It's important to consider that benzeneseleninic acid **31** can itself be oxidized by H_2O_2 to form benzeneperoxyseleninic acid **32**. This species can thereupon oxidize **23** or **24**, triggering an autocatalytic mechanism in the second part of the whole process. The oxidation of **23** by **32** has an activation energy of +8.1 kcal mol^{-1} and an overall reaction energy of –30.3 kcal mol^{-1}, leading to the formation of **24** and **31**. In comparison with the oxidation of **23** by **26**, this step is much more favorable energetically (Scheme S2 I); this suggests that the autocatalytic behavior observed is due to benzeneperoxyseleninic acid and can be established only once it is formed, that is in the later stage of the whole process. This would explain why the kinetic profile suddenly becomes sigmoidal, and also the sharp acceleration in the rate at which **24** diminishes (Figure 5 (f)).

Oxidation of PhSeSePh

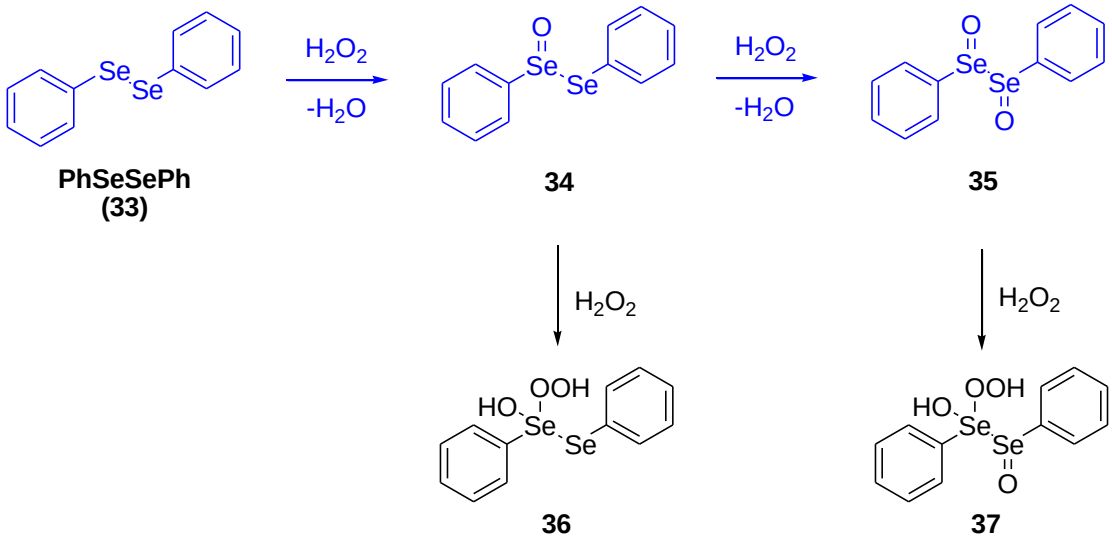

Scheme 6 Mechanism of oxidation of **PhSeSePh** by H_2O_2. The direct oxidation step is shown in blue.

An important feature of **PhSeSePh** is the presence of a direct Se-Se bond, which, being substantially weaker than the Se-C bond, [34] may break upon oxidation. The ^{1}H–^{77}Se HMBC of **33**

presents, as expected, a correlation with the proton in ortho, split as a doublet in the proton dimension and at a selenium chemical shift of 456 ppm (Figure 6 (a)).

Depending on the orientation of the phenyl rings, the computed ^{77}Se chemical shift varies from 388.1 ppm (local minimum when both phenyl rings are perpendicular to the Se–Se bond) to 593.9 ppm (local minimum when both phenyl rings are in the plane defined by the Se–Se–C angle). This confirms, as reported in previous studies, that the orientation of the phenyl rings has a strong influence upon the chemical shift value. For a more extensive discussion on this conformational flexibility and its significant effect on the ^{77}Se chemical shift, the curious reader is referred to a recently published paper by some of us, [45] as well as others. [46]

Upon oxidation by H_2O_2, the selenium resonance becomes strongly down-field shifted at a frequency of 1169 ppm (Figure 6 (b)). This is significantly higher than expected for a selenoseleninate and corresponds to the formation the seleninic acid **31**, in agreement with reports by other authors. [47] HRMS analysis confirmed the identity of the reaction product **31** (m/z 188.94, Figure S4).

10.1002/chem.201604915

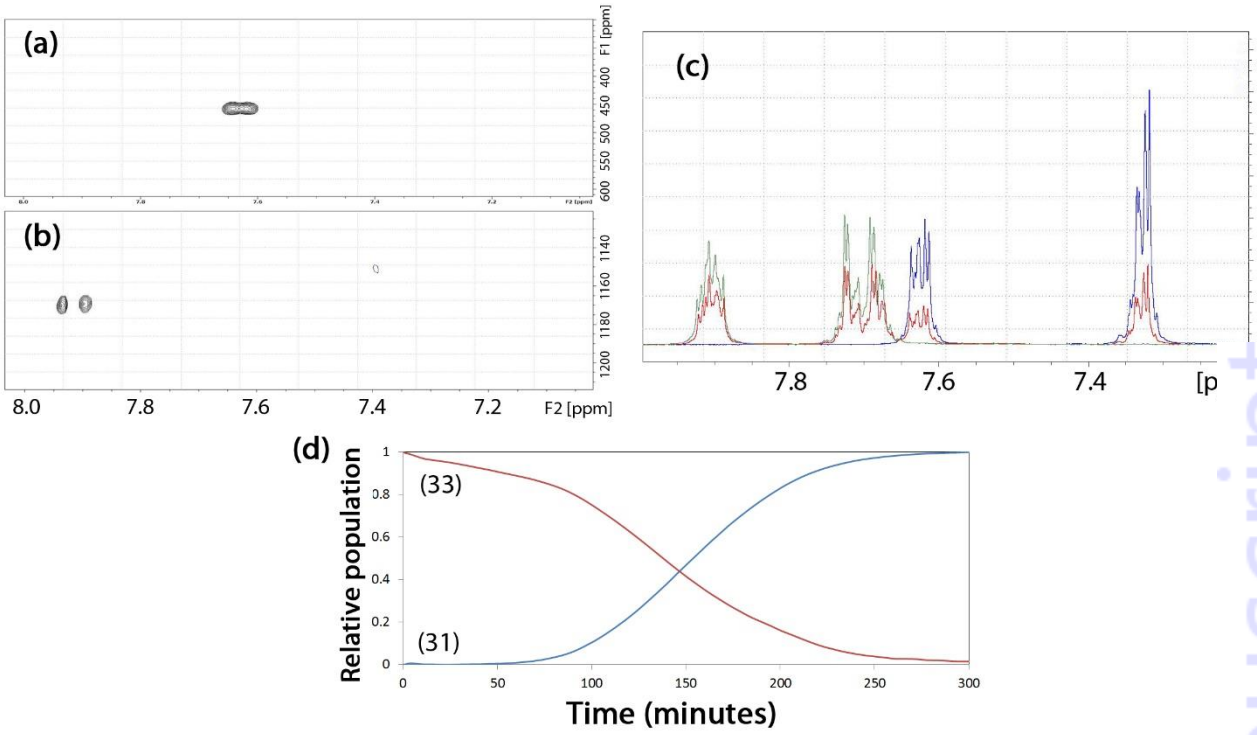

Figure 6. Experimental characterization by NMR of **PhSeSePh** (10mM) oxidation by 3 equivalents of H_2O_2: ^{77}Se-HMBC of reduced **PhSeSePh** (a) and oxidized product obtained upon addition of H_2O_2 (b). Representative changes in the ^{1}H-NMR spectra acquired after 4 (blue), 167 (red), and 278 minutes (green) from the addition of H_2O_2 are shown in (c). The normalized areas of selected NMR signals have been used to derive the kinetic profile represented in (d); the kinetic curves are labeled with the compound numbers used in the text.

The reagent **33** and the final product **31** are each characterized by two distinct multiplets in the aromatic region of ^{1}H NMR spectrum (Figure 6 (c)), which luckily do not overlap making it possible for us to follow the kinetics of the oxidation of **33** by H_2O_2. This kinetic profile (Figure 6 (d)) has the feature of an inverse sigmoidal relation between the reactants and products, very different from the plots of **PhSe(n-Bu)** and **PhSeMeSePh**. An interesting comparison may be drawn with **PhSeEtSePh**, whose late stages somewhat resemble this sigmoidal relationship. After a relative long lag-phase lasting around 1 hour the NMR signals of **33** started to decrease rapidly with the simultaneous appearance of new multiplets that were assigned to the seleninic acid **31** by HRMS analysis. This suggests that the direct oxidation of the **PhSeSePh** by H_2O_2 is a relative slow process followed by a rapid step in which the oxidized product acts as a catalyst for the first step of the reaction. We investigated this hypothesis via a computational approach.

10.1002/chem.201604915

For **33**, the first reaction with H_2O_2 via a reaction barrier of +19.1 kcal mol^{-1} and with a reaction energy of –38.1 kcal mol^{-1}, leads to the formation of the singly oxidized product **34**. Subsequent reaction with a second equivalent of H_2O_2 may form the doubly oxidized species **35** with a choice of two pathways: one leading to (*R*,*R*)-**35**, and the other to (*R*,*S*)-**35**. The latter is found to proceed via a slightly lower reaction barrier (+18.9 kcal mol^{-1} vs. +19.4 kcal mol^{-1}) and leads to products with greater stability (–38.3 kcal mol^{-1} vs. –35.3 kcal mol^{-1}). First we explored whether an autocatalytic pathway, revealed by the sigmoidal shape of the kinetics, might be triggered by the formation of a hydroxy perhydroxy species.

Both the diselenide species and the monoselenide species, which results from Se–Se bond rupture, can be involved in the autocatalytic process; we return to this latter possibility later. In the autocatalytic mechanism involving the diselenide, the mono-oxidized product **34** can react with 1 equivalent of H_2O_2 to form the hydroxy perhydroxy species **36**. For this reaction, a transition state has been located at an energy of +14.7 kcal mol^{-1}, leading to products at +12.5 kcal mol^{-1}. A second possible TS, in which the incoming H_2O_2 approaches at a different angle, is more than 7 kcal mol^{-1} higher in energy, indicating that the conformations of stationary points and transition states must be carefully considered for these compounds. The reactions involving the hydroxy perhydroxy species **36** and **37** are shown and commented in the Supporting information (Scheme S3); also in this case the energy values show a favorability of the direct oxidation mechanism (**33** to **34** and **34** to **35**).

10.1002/chem.201604915

I.

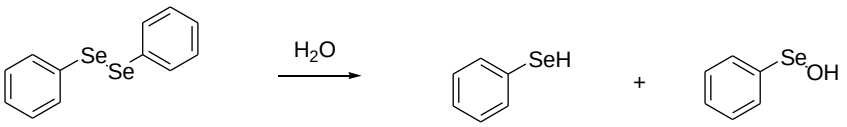

PhSeSePh (33) **38** **29**

II.

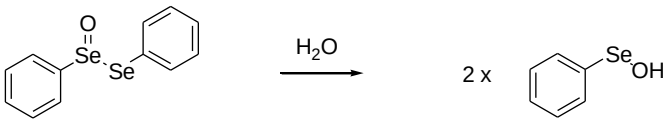

34 **29**

III.

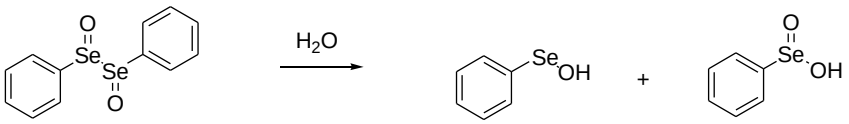

35 **29** **31**

IV.

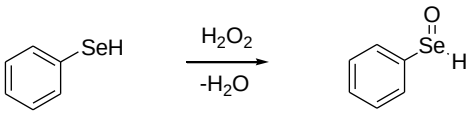

38 **39**

V.

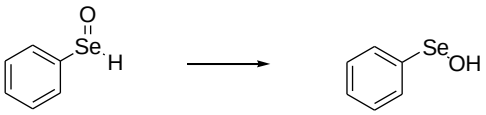

39 **29**

VI.

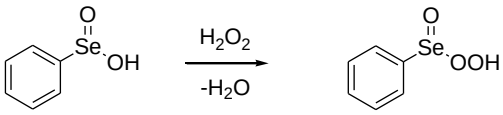

31 **32**

VII.

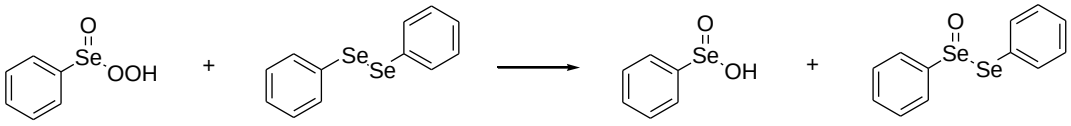

32 **PhSeSePh (33)** **31** **34**

VIII.

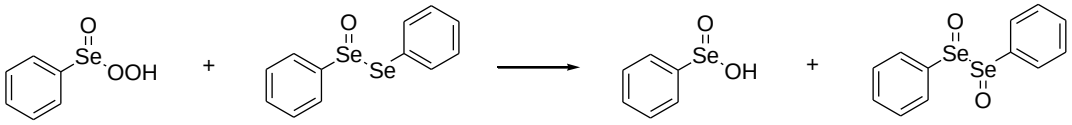

32 **34** **31** **35**

Scheme 7. Reactions considered for **PhSeSePh** (**32**) involved in, or after, Se–Se bond rupture, including labels (in bold) for relevant molecular species.

As benzeneseleninic acid **31** is the observed final product, we have considered several reactions that include cleavage of the Se–Se bond, and a possible autocatalytic mechanism that may follow. These reactions are collected in Scheme 7. In reactions I-III, the Se–Se bond breaks, and two monoselenides are formed upon the assumption that water is involved in the process and readily available. Locating transition states has not been attempted for these reactions, but their reaction energies are calculated to be +28.3 kcal mol^{-1}, +12.2 kcal mol^{-1} and +1.2 kcal mol^{-1}, respectively. This trend, which is likely due to a decrease in the Se–Se bond strength upon subsequent oxidations, implies that it is more probable for Se–Se bond cleavage to occur after the second oxidation.

Each monoselenide formed after Se–Se bond cleavage can be transformed into the benzeneseleninic acid **31**. For phenyl selenol (**38**), this involves a reaction with H_2O_2 to form **39** (reaction IV: $\Delta E^{\ddagger}$ = +22.5 kcal mol^{-1}, ΔE = –28.1 kcal mol^{-1}), which can rearrange to the phenyl selenenic acid **29** (reaction V: $\Delta E^{\ddagger}$ = +30.9 kcal mol^{-1}, ΔE = –26.1 kcal mol^{-1}). From **29** the benzeneseleninic acid **31** can be generated, as discussed above ($\Delta E^{\ddagger}$ = +12.6 kcal mol^{-1}, ΔE = –49.2 kcal mol^{-1}).

Upon formation of the benzeneseleninic acid an autocatalytic pathway can again be initiated, which starts with the conversion of the seleninic acid into the perhydroxy compound **32**. For this step (reaction VI), a somewhat high-energy transition state at +24.8 kcal mol^{-1} and a reaction energy of –5.5 kcal mol^{-1} have been computed. **32** can then act as an oxidant towards **33** and **34** (reactions VII and VIII) in a way similar to the hydroxy perhydroxy compounds considered in some of the reactions in Scheme S3, except now a hydroxy group is formed. No water is expelled, because of the presence of a doubly-bonded oxygen in the reactant **32**, instead of the hydroxy group in, for example, **36**.

10.1002/chem.201604915

Guided by the results obtained for the other compounds, for which an autocatalytic process mediated by the hydroxy perhydroxy selenane is not energetically feasible (however, we have not excluded the possibility), an investigation has been conducted into the possibility that the benzeneperoxyseleninic acid **32** is an active catalyst within this mechanism. Also a recent hypothesis by Sancineto et al.[48] proposes that **32** may be reduced to **31** with a concurrent oxidation of a substrate; which in this specific case is **PhSeSePh** itself (Scheme 8). This might indeed trigger an autocatalytic process accelerating the reaction until the substrate is completely oxidized, or the H_2O_2 is consumed. For reaction VII, in which **32** reacts with the starting compound **33**, a rather low reaction barrier of +11.8 kcal mol^{-1} and a reaction energy of –32.6 kcal mol^{-1} are obtained. For reaction VIII, a similar reaction energy of –32.8 kcal mol^{-1} is computed; here the only TS found is analogous to that found for the direct oxidation from **34** to **35**, but with the benzeneperoxyseleninic species instead of H_2O_2, in which no hydrogen transfer to the doubly-bonded oxygen takes place. The relative energy of this TS is +11.4 kcal mol^{-1}, indicating that this mechanism might also be viable. Indeed, the oxidation by **32** is energetically favored over the oxidation by H_2O_2, as found with **PhSeEtSePh**, justifying the onset of autocatalysis after a slow initial oxidation by H_2O_2.

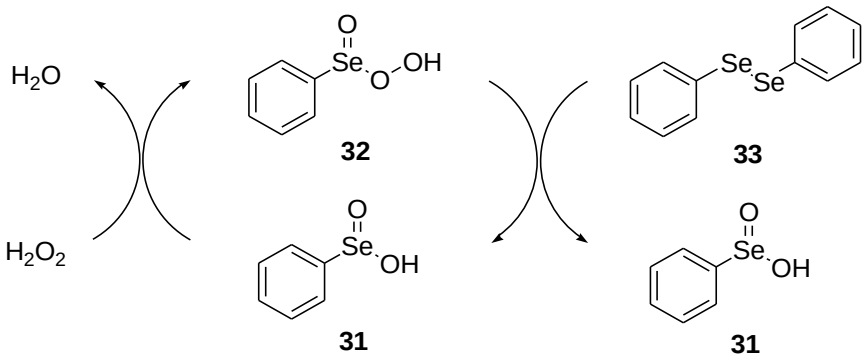

Scheme 8. Autocatalytic oxidation of **PhSeSePh**.

10.1002/chem.201604915

Conclusions

With the aim of providing rational insights into the reactivity of organic selenides towards H_2O_2, we considered four model compounds in this combined experimental and computational study. These compounds can be assigned to three classes: (i) alkyl aryl selenides (**PhSe(n-Bu)**), (ii) bis(phenylselanyl)alkanes (**PhSeMeSePh** and **PhSeEtSePh**) and (iii) diaryl diselenides (**PhSeSePh**). The mechanistic investigation was designed to demonstrate the role of a mutual influence from selenium atoms in the formation of the oxidation product. The proposed mechanisms were supported by a combination of quantitative experimental techniques (NMR), assessment of the identity of reaction products and detectable intermediates by HRMS, and quantum chemistry modeling. The major outcomes of our analysis are: (i) all of the studied selenides undergo oxidation by H_2O_2, possessing comparable activation energies (all below 20 kcal mol^{-1}). Further oxidation also occurs, leading to diselenoxides in the dinuclear compounds; (ii) hydroxy perhydroxy Se derivatives, formed upon further oxidation of selenoxide moieties by H_2O_2 in a thermodynamically unfavored process, appear to be worse oxidants than H_2O_2 towards selenides, and thus are not able to trigger an autocatalytic mechanism. Nevertheless, as reported in literature,[2,43] they may indeed be efficient *in situ* generated oxidants for specific organic reactions, explaining the catalytic key role of selenides; (iii) the oxidation of **PhSeSePh** by H_2O_2 clearly exhibits autocatalytic behavior, but cleavage of the Se-Se bond opens numerous different pathways, making mechanistic analyses more complex in nature. Autocatalysis via hydroxy perhydroxy Se species formed, before as well as after Se-Se bond rupture, is excluded based on the computed energetics. However, autocatalysis via the benzeneperoxyseleninic acid, which forms upon oxidation by H_2O_2 of the seleninic acid (the main product from oxidation of **PhSeSePh** by H_2O_2), seems to be a feasible proposition, since its energetics are more efficient than H_2O_2 in oxidizing selenides; (iv) as further support to the conclusions outlined in (iii), evidence for autocatalysis is also found in the final stages of the oxidation of **PhSeEtSePh** at the time when seleninic acid is formed by an elimination side reaction.

10.1002/chem.201604915

This species is readily oxidized by H_2O_2 generating benzeneperoxyseleninic acid which can oxidize the diselenide substrate, triggering an autocatalytic mechanism. Energy profiles related to all of these outcomes are shown in Figure 7.

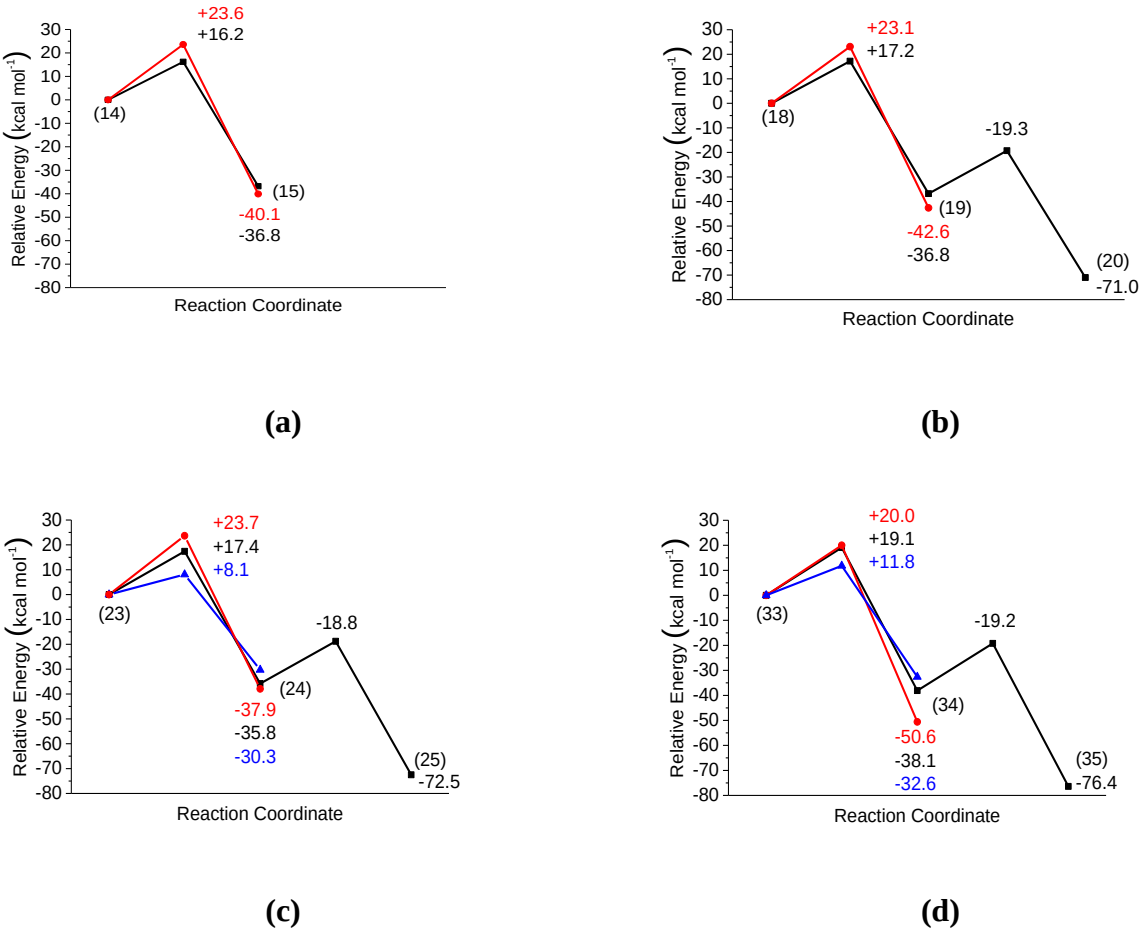

Figure 7. Energy profiles for the oxidation of **PhSe(n-Bu)** (a), **PhSeMeSePh** (b), **PhSeEtSePh**, (c) and **PhSeSePh** (d) by H_2O_2 (black), hydroxy perhydroxy derivative (red) and benzeneperoxyseleninic acid (blue); level of theory: scalar-ZORA-OLYP/TZ2P-sc; all values of each curve are relative to the energies of the corresponding free reactants.

In conclusion, similarity is found in the behavior of **PhSe(n-Bu)** and **PhSeMeSePh**, which through oxidation to the hydroxy perhydroxy selenium derivatives, guarantee the *in situ* generation of an oxidant superior to H_2O_2. A different similarity is outlined for **PhSeEtSePh** and **PhSeSePh**, wherein their oxidation leads, through different paths, to the formation of the seleninic acid derivative, which is easily oxidized to benzeneperoxyseleninic acid, triggering an autocatalytic mechanism. In addition to this, we have assessed that hydroxy perhydroxy derivatives are less

efficient in the oxidation of selenides, while the benzeneperoxyseleninic acid is more efficient in oxidizing selenides in comparison to hydrogen peroxide. Notably, the lowest reaction barriers are always accompanied by the least stable products (Figure 7), an energetic feature that is optimal when these oxidation steps are inserted into catalytic cycles.[49]

Our combined NMR and computational analysis confirms the plausible mechanistic paths through which mono and diselenides mediate oxidation by H_2O_2 within organic reactions, a process whose occurrence is otherwise unfavorable. As a guide in choosing a Se catalyst for an organic reaction, we suggest an investigation into the efficiency of both hydroxy perhydroxy species and the the benzeneperoxyseleninic acid in the oxidation step of the process in question. If benzeneperoxyseleninic acid is found to be more efficient, the choice can only fall back on the very popular **PhSeSePh**.

Acknowledgements

This research has been funded by Università degli Studi di Padova (CPDA127392/12). The calculations were carried out on Galileo at CINECA (Casalecchio di Reno, Italy) thanks to the ISCRA grant NAMASTÉ (*NMR Assisted Molecular Analysis: Selenium and Tellurium Enzyme mimics*, 2015, PI: Laura Orian) and on the computational facilities of C3P at Dipartimento di Scienze Chimiche (Università degli Studi di Padova). Elena Vialetto and Marco Prevedello are acknowledged for contribution in preliminary calculations carried out during their Bachelor thesis internship at DiSC (Università degli Studi di Padova). G. Zagotto, M. Bellanda and L. Orian are grateful to Prof. Georg Schreckenbach (University of Manitoba, Canada) for enlightening comments on the NMR analysis.

References

[1] (a) Organoselenium Chemistry: Between Synthesis and Biochemistry; Santi, C., Ed.; Bentham, 2014. (b) G. Mugesh, W. -W. du Mont, H. Sies, *Chem. Rev.* **2001**, *101*, 2125−2180.

[2] J. D. Woollins, R. S. Laitinen, Eds. Selenium and Tellurium Chemistry From Small Molecules to Biomolecules and Materials, Chap. 11 Springer Verlag: Berlin, Heidelberg, 2011.

[3] (a) D. M. Freudendahl, S. A. Shahzad, T. Wirth, *Eur. J. Org. Chem.* **2009**, *11*, 1649−1664; (b) D. M. Freudendahl, S. Santoro, S. A. Shahzad, C. Santi, T. Wirth, *Ang. Chemie Int. Ed.* **2009**, *11*, 1649−1664; (c) S. Santoro, J. B. Azeredo, V. Nascimento, L. Sancineto, A. L. Braga, C. Santi, *RSC Adv.* **2014**, *4*, 31521−31535; (d) C. Santi, S. Santoro, B. Battistelli, *Curr. Org. Chem.* **2010**, *14*, 2442−2462; (e) T. Back, *Can. J. Chem.* **2009**, *87*, 1657−1674.

[4] (a) J. T. Rotruck, A. L. Pope, H. E. Ganther, A. B. Swanson, D. G. Hafeman, W. G. Hoekstra, *Science* **1973**, *179*, 588–590; (b) L. Flohe´, W. A. Gunzler, H. H. Schock, *FEBS Lett.* **1973**, 32, 132–134.

[5] (a) L. Orian, P. Mauri, A. Roveri, S. Toppo, L. Benazzi, V. Bosello-Travain, A. De Palma, M. Maiorino, G. Miotto, M. Zaccarin, A. Polimeno, L. Flohé, F. Ursini, *Free Radic. Biol. Med.* **2015**, *87*, 1–14; (b) R. Prabhakar, T. Vreven, K. Morokuma, D. G. Musaev, *Biochem.* **2005**, *44*, 11864−11871.

[6] J. D. Woollins, R. S. Laitinen, Eds. Selenium and Tellurium Chemistry From Small Molecules to Biomolecules and Materials, Chap. 12 Springer Verlag: Berlin, Heidelberg, 2011.

[7] H. J. Reich, R. J. Hondal. *ACS Chem. Biol*. **2016**, *11*, 821−841.

[8] C. W. Nogueira, G. Zeni, J. B. T. Rocha, *Chem. Rev.* **2004**, *104*, 6255−6285.

[9] (a) A. Wendel, M. Fausel, H. Safayhi, G. Tiegs, R. Otter, *Biochem. Pharmacol.* **1984**, *33*, 3241−3245; (b) A. Muller, E. Cadenas, P. Graf, H. Sies, *Biochem. Pharmacol.* **1984**, *33*, 3235−3239.

[10] L. P. Wolters, L. Orian, *Curr. Org. Chem.* **2016**, *20*, 189−197.

[11] S. Antony, C. A. Bayse, *Inorg. Chem*. **2011**, *50*, 12075-12084.

[12] K. Goto, T. Saiki, R. Okazaki, *Phosphorous, sulphur and silicon* **1998** *136*, 475–478.

[13] L. Orian, S. Toppo, *Free Rad. Biol. Med.* **2014**, *66*, 65−74.

[14] M. Iwaoka, S. Tomoda, *J. Am. Chem. Soc*. **1994,** *116*, 2557–2561.

[15] G. S. Heverly-Coulson, R. J. Boyd, *J. Phys. Chem. A* **2010** *114*,1996–2000.

[16] (a) M. Ibrahim, W. Hassan, D. F. Meinerz, M. dos Santos, C. V. Klimaczewski, A. M. Deobald, M. S. Costa, C. W. Nogueira, N. B. V. Barbosa, J. B. T. Rocha, *Mol. Cell. Biochem.* **2012**, *371*, 97–104**;** (b) I. J. Kade, M. W. Paixao, O. E. D. Rodrigues, N. B. V. Barbosa, A. L. Braga, D. S. Avila, C. W. Nogueira, J. B. T. Rocha, *Neurochem. Res.* **2008**, *33*, 167–178; (c) I. J. Kade, J. B. T. Rocha, *J. Appl. Toxico*l. **2010**, *30*, 688–693; (d) W. Hassan, J. B. T. Rocha, *Molecules* **2012**, *17*, 12287−12296; (e) D. F. Meinerz, J. Allebrandt, D. O. C. Mariano, E. P. Waczuk, F. A. Soares, W. Hassan, J. B. T. Rocha, *PeerJ* **2014,** 290.

[17] J. W. Chu, B. L. Trout, *J. Am. Chem. Soc.* **2004**, *126*, 900−908.

[18] S. R. Wilson, P. A. Zucker, R. R. C. Huang, A. Spector, *J. Am. Chem. Soc.* **1989**, *111*, 5936−5939.

[19] S. R. Walker, W. Jiao, E. J. Parker, *Bioorg. Med. Chem. Lett.* **2011**, *21(17)*, 5092−5097.

[20] L. Syper, J. Mlochowski, *Synthesis* **1984**, *5*, 439−442.

[21] K. Ajiki, M. Hirano, K. Tanaka, *Org. Lett.* **2005**, *7(19)*, 4193−4195.

[22] H. J. Reich, S. K. Shah, F. Chow *J. Am. Chem. Soc.* **1979**, *101*, 6638−6648.

[23] D. J. Gulliver, E. G. Hope, W. Levason, S. G. Murray, D. M. Potter, G. L. Marshall *J. Chem. Soc., Perkin Trans. 2* **1984**, *3*, 429−434.

[24] O. Prakash, P. Singh, G. Mukherjee, A. K. Singh *Organometallics* **2014**, *33(4)*, 983–993.

[25] R.E. Hurd, B. K. John *J. Magn. Reson*. **1991**, *91*, 648−653.

[26] D.J. Press, T. G. Back *Org. Lett.* **2011**, *13(15)*, 4104−4107.

[27] (a) G. te Velde, F. M. Bickelhaupt, E. J. Baerends, C. Fonseca Guerra, S. J. A. van Gisbergen, J. G. Snijders, T. Ziegler, *J. Comput. Chem.* **2001**, *22*, 931−967; (b) C. Fonseca Guerra, J. G. Snijders, G. te Velde, E. J. Baerends, *Theor Chem. Acc.* **1998**, *99*, 391−403; (c) E. J. Baerends, T.

Ziegler, J. Autschbach, D. Bashford, A. Bérces, F. M. Bickelhaupt, C. Bo, P. M. Boerrigter, L. Cavallo, D. P. Chong, L. Deng, R. M. Dickson, D. E. Ellis, M. van Faassen, L. Fan, T. H. Fischer, C. Fonseca Guerra, M. Franchini, A. Ghysels, A. Giammona, S. J. A. van Gisbergen, A. W. Götz, J. A. Groeneveld, O. V. Gritsenko, M. Grüning, S. Gusarov, F. E. Harris, P. van den Hoek, C. R. Jacob, H. Jacobsen, L. Jensen, J. W. Kaminski, G. van Kessel, F. Kootstra, A. Kovalenko, M. V. Krykunov, E. van Lenthe, D. A. McCormack, A. Michalak, M. Mitoraj, S. M. Morton, J. Neugebauer, V. P. Nicu, L. Noodleman, V. P. Osinga, S. Patchkovskii, M. Pavanello, P. H. T. Philipsen, D. Post, C. C. Pye, W. Ravenek, J. I. Rodríguez, P. Ros, P. R. T. Schipper, H. van Schoot, G. Schreckenbach, J. S. Seldenthuis, M. Seth, J. G. Snijders, M. Solà, M. Swart, D. Swerhone, G. te Velde, P. Vernooijs, L. Versluis, L. Visscher, O. Visser, F. Wang, T. A. Wesolowski, E. M. van Wezenbeek, G. Wiesenekker, S. K. Wolff, T. K. Woo, A. L. Yakovlev, *ADF2014, SCM, Theoretical Chemistry*; Vrije Universiteit: Amsterdam, The Netherlands; http://www.scm.com/.

[28] (a) M. Swart, F. M. Bickelhaupt, Computer software (QUILD). Vrije Universiteit: Amsterdam, The Netherlands, 2006; b) M. Swart, F. M. Bickelhaupt, *Int. J. Quantum Chem.* **2006**, *106*, 2536−2544; c) M. Swart, F. M. Bickelhaupt, *J. Comput. Chem.* **2008**, *29*, 724−734.

[29] (a) A. D. Becke, *J. Chem. Phys.* **1988**, *88*, 2547–2553; (b) M. Franchini, P. H. T. Philipsen, L. Visscher, *J. Comput. Chem.* **2013**, *34*, 1819–1827.

[30] E. van Lenthe, E. J. Baerends, *J. Comput. Chem.* **2003**, *24*, 1142−1156.

[31] (a) E. van Lenthe, E. J. Baerends, J. G. Snijders, *J. Chem. Phys.* **1993**, *99*, 4597−4610; (b) E. van Lenthe, E. J. Baerends, J. G. Snijders, *J. Chem. Phys.* **1994**, *101*, 9783–9792; (c) E. van Lenthe, R. van Leeuwen, E. J. Baerends, J. G. Snijders, *Int. J. Quantum Chem.* **1996**, *57*, 281–293.

[32] G. Schreckenbach, T. Ziegler, *J. Phys. Chem.* **1995**, *99*, 606–611.

[33] (a) M. Swart, A. W. Ehlers, K. Lammertsma, *Mol. Phys.* **2004**, *102*, 2467−2474; (b) N. C. Handy, A. Cohen, *J. Mol. Phys.* **2001**, *99*, 403−412; (c) J. P. Perdew, K. Burke, M. Ernzerhof, *Phys. Rev. Lett.* **1996**, *77*, 3865−3868.

[34] F. Zaccaria, L. P. Wolters, C. Fonseca Guerra, L. Orian, *J. Comp. Chem.* **2016**, *37*, 1672−1680.

[35] G. Schreckenbach, *J. Chem. Phys*. **1999**, *110*, 11936.

[36] N. C. Handy, A. J. Cohen, *J. Chem. Phys.* **2002**, *116*, 5411−5418.

[37] (a) A. P. Bento, M. Solà, F. M. Bickelhaupt, *J. Comput. Chem.* **2005**, *26*, 1497−1504; (b) A. P. Bento, M. Solà, F. M. Bickelhaupt, *J. Chem. Theory Comput.* **2008**, *4*, 1445−1445.

[38] M. Bortoli, L. P. Wolters, L. Orian, F. M. Bickelhaupt *J. Chem. Th. Comp.* **2016**, *12*, 2752−2761.

[39] (a) A. Bérces, R. M. Dickson, L. Fan, H. Jacobsen, D. Swerhone, T. Ziegler, *Comput. Phys. Commun.* **1997**, *100*, 247−262. (b) H. Jacobsen, A. Bérces, D. Swerhone, T. Ziegler, *Comput. Phys Commun.* **1997**, *100*, 263−276. (c) S. K. Wolff, *Int. J. Quantum Chem.* **2005**, *104*, 645−659.

[40] C. Bayse, *Inorg. Chem.* **2004**, *43*, 1208−1210.

[41] (a) M. Bühl, W. Thiel, U. Fleischer, W. Kutzelnigg, *J. Phys. Chem.* **1995**, *99*, 4000−4007; (b) D. B. Chesnut, *Chem. Phys.* **2004**, *305*, 237−241.

[42] H. Duddek, *Prog. Nucl. Magn. Reson. Spectrosc*. **1995**, *27*, 1−323.

[43] (a) M. A. Goodman, M. R. Detty, *Organometallics* **2004**, *23*, 3016-3020; (b) V. Nascimento, E. E. Alberto, D. W. Tondo, D. Dambrowski, M. R. Detty, F. Nome, A. L. Braga, *J. Am. Chem. Soc.*, **2012**, *134*, 138-141.

[44] N. Kunieda, J. Nokami, M. Kinoshita, *B. Chem. Soc. Jpn.* **1976**, *49(1)*, 256−259.

[45] M. Torsello, A. C. Pimenta, L. P. Wolters, I. S. Moreira, L. Orian, A. Polimeno. *J. Phys. Chem. A* **2016**, *120*, 4389−4400

[46] (a) W. Nakanishi, S. Hayashi, D. Shimizu, M. Hada, *Chem. Eur. J.* **2006**, *12*, 3829−3846. (b) W. Nakanishi, S. Hayashi, M. Hada. *Chem. Eur. J.* **2007**, *13*, 5282−5293.

[47] K. L. House, R. B. Dunlap, J. D. Odom, Z.-P. Wu, D. Hilvert, *J. Am. Chem. Soc.* **1992**, *114(22)*, 8573−8579.

[48] L. Sancineto, C. Tidei, L. Bagnoli, F. Marini, E. J. Lenardao, C. Santi, *Molecules* **2015**, *20*, 10496−10510

[49] C. Amatore, A. Jutand, *J. Organomet. Chem.* **1999**, *576*, 254−278.

10.1002/chem.201604915

FOR TABLE OF CONTENTS USE ONLY